Geochemical characteristics of orthopyroxene-bearing metamorphosed lithologies in the northern Chilka lake area, Eastern Ghats belt, India: Insights into the original nature and petrogenesis of precursors

Joel George[1*]

[1]School of Earth, Ocean and Climate Sciences, Indian Institute of Technology, Bhubaneswar, Argul, Khordha -752050

*Corresponding author. Email: george.joel9@gmail.com

Abstract

The northern Chilka Lake area stone quarries expose a high-grade terrane comprising a metapelitic suite interbanded with orthopyroxene-bearing gneisses and garnet-biotite leucogneisses (leptynites). This study presents bulk-rock and mineral chemistry data of the orthopyroxene-bearing units to evaluate the true nature of their protoliths and to comment on their petrogenesis. Field, petrographic, and geochemical observations reveal three distinct variants: Enderbitic paragneisses (EP), Garnetiferous Charnockites (G-Ch), and Non-Garnetiferous Charnockites (NG-Ch). Orthopyroxenes in each unit are texturally and compositionally distinct, and highly likely of metamorphic origin. A detailed study of the EPs suggests that their field and chemical characteristics are more consistent with a depositional origin rather than an intrusive one. Based on bulk rock geochemical aspects of non-migmatitic samples, a provenance involving both felsic and mafic-ultramafic rocks is speculated for the unit. Under this interpretation, the ‘ultramafic two-pyroxene granulite xenoliths’ previously reported to be within this unit possibly represent lithic fragments from an ultramafic source, thereby likely reflecting the very low transport distance of some of the additions to the unit. In contrast, the G-Ch likely represent disequilibrium melts derived from the metapelitic suite in the region, with their slightly higher Fe, Ca, Mg, Nb, Ti, Eu, and Sr contents compared to leptynites possibly linked to restite entrainment. As G-Ch rocks rarely exist with the prevalent metapelitic suite as wallrocks, it is deduced from field evidence that the melts migrated away from source region just like the leptynite precursors. The NG-Ch rocks, with their characteristic HREE+Y depletion, negative Nb, Ti anomalies and high Sr are most likely products of partial melting of predominantly granodioritic component of a lower crustal TTG gneiss. This study therefore highlights the complexity of the metasedimentary units in the Chilka lake area and reaffirms earlier interpretations regarding the presence of a metagreywacke unit, which may be as predominant as the already recognized metapelite unit. Along with that, this study also suggests the presence of two distinct granitoids of igneous origin, which, although undated, are interpreted to be products of crustal reworking during the Grenvillian orogeny.

Keywords: orogenic belt; orthopyroxene; protolith; granulite; partial melting; crustal reworking; Chilka lake

1. Introduction

Orogenic belts preserve evidence of crustal processes operating at convergent settings. The Eastern Ghats belt is a Precambrian orogenic belt that was has witnessed intense deformation, high-grade metamorphism, and crustal anatexis. (Dobmeier and Raith, 2003 and references therein). As orogens are prime locations of crustal reworking, it is highly challenging at times to understand the true nature of rock units but attempts in this direction via interpretation of robust geochemical and isotopic data have been shown to be effective. (Rickers et al., 2001) (Bose et al., 2011b) (Bhattacharya et al., 2012) (Sarkar et al., 2015)

Interestingly, as the Chilka lake area in the northern part of the Eastern Ghats belt is widely known for its preservation of deformational imprints, more emphasis has been given to the structural and metamorphic aspects of the terrane (Bhattacharya et al., 1993,1994) (Sen et al., 1995) (Dobmeier and Raith,2000) (Dobmeier and Simmat, 2001) (Bose et al., 2012) (Bose et al., 2016) such that the precise details of the petrogenetic aspects of the units in the region, especially the variants of orthopyroxene-bearing units, have been largely understudied. Apart from the petrogenetic studies conducted on the leucogneisses (Sen and Bhattacharya, 1997), anorthosites (Chakrabarti et al., 2011), mafic granulites (Bose et al., 2011b), metapelitic suite (Bhattacharya et al., 2012) and a migmatitic variant of orthopyroxene-bearing felsic gneisses(OFGs) (Bose et al., 2020) in the Chilka lake area, a detailed study of the petrogenetic aspects of the precursors to all the variants of orthopyroxene-bearing gneisses that exists as bands/lenses within the larger leucogranitoids and metapelitic units is yet to be undertaken.

This study presents a geochemical investigation of orthopyroxene-bearing units in the northern Chilka Lake area to evaluate the petrogenesis of their precursors. The findings are used to better understand the history of the terrane. Since the units have undergone significant metamorphism, behavior of the LILEs has been examined to evaluate the effects of metamorphism and the petrogenetic aspects of the rock suites have been commented upon solely in light of coherent immobile element chemistry.

2. Geological Setting

The Chilka lake area in the northern part of the Eastern Ghats belt hosts a group of intensely metamorphosed rock suites that include a metapelitic suite (comprising mainly khondalites and minor calc-granulites and quartzites), orthopyroxene-bearing units (both massive and localized) of varying compositions, meta-leucogranitoids (leptynites), minor mafic granulites and an anorthosite massif. (Bhattacharya et al., 1993, 1994) (Sen and Bhattacharya, 1997) (Dobmeier and Raith, 2000). According to the domain classification based on mantle model ages, the Chilka Lake area falls under Domain 3, which is interpreted to encompass rocks derived from the reworking of largely homogeneous Proterozoic material, as per studies on khondalites, charnockites, and leptynites (Rickers et al., 2001). The geodynamic history of the area has been interpreted to be predominantly collisional (Rickers et al., 2001; Dasgupta et al., 2013), with the earliest of the major deformation events (D1) understood to have occurred between ~1250 and 1100 Ma (Simmat and Raith, 2008). The peak of subsequent deformation event (D2), which imparted the pervasive S2 foliation to units in the region has been dated ~990Ma (Bose et al., 2016).

The original nature of the metapelitic suite that is identified to preserve the S1 foliation associated with the earliest deformation event was interpreted as a shale-greywacke sedimentary sequence, similar to marine turbidites (Sen and Bhattacharya, 1997; Bhattacharya et al., 2012), and the leptynites were interpreted to have formed by mica dehydration melting of the metapelitic suite during a granulite facies metamorphic event, which is argued to have occurred during D2 (Sen and Bhattacharya, 1997). Both the mafic granulite and anorthosite precursors have been independently interpreted as mantle-derived units based on their respective geochemical characteristics, with their emplacement possibly linked to Rodinia break-up (Bose et al., 2011b; Chakrabarti et al., 2011).

When it comes to the orthopyroxene-bearing units, both of the first two major studies (Bhattacharya et al., 1993, 1994; Dobmeier and Raith, 2000) suggested that they likely represent igneous granitoids that later underwent granulite facies metamorphism. However, the classification of the orthopyroxene-bearing units as ‘charnockites’ by (Bhattacharya et al., 1993, 1994) was later challenged by (Dobmeier and Raith 2000), wherein they argued that the modal volume of plagioclase in these units makes ‘enderbite’ a more appropriate term. More recently, (Bose et al. 2020) suggested that a variant of orthopyroxene-bearing gneisses in the region is plausibly a paragneiss, formed after metamorphism and partial melting of a greywacke-type protolith. In the light of such findings, a comprehensive study of the geochemical characteristics of all the orthopyroxene bearing units in this region is necessary to obtain a complete picture of the compositional variations.

3. Field and petrographic features of orthopyroxene-bearing units

The present study region encompasses active stone quarries exposed in the northern part of Chilka lake area, in a region locally known as Tapang. Thorough field studies were conducted in four stone quarries in the region namely, USIS Chowk Quarry, Greenlake Quarry, Hatia Quarry and Calcutta Quarry (Fig 1b). This study follows the location names originally introduced by (Dobmeier and Raith 2000), with the addition of a new quarry, Greenlake. The field aspects and petrographic studies of representative samples confirmed the presence of the following orthopyroxene bearing entities in the region:

3.1 *Enderbitic paragneisses (EP)*

The most predominant member of the orthopyroxene bearing group in the study region that is characterized by its melanocratic and fine-grained nature. It occurs as centimeter to meter scale bands within khondalites and leptynites (Fig 2a and c). Upon close inspection, its bandings are visible. Petrographic studies did indicate a higher modal proportion of plagioclase feldspar as previously reported by (Dobmeier and Raith, 2000), (Fig 4a). The petrographic study also revealed that a few highly plagioclase rich varieties having no alkali-feldspar or quartz are present in the region. Representative samples of each variant of the unit has been plotted on the QAP plot (Frost and Frost, 2008) (Fig 4a). For reference, the average modal proportions of the unit as reported by (Dobmeier and Raith, 2000) has also been included. The mineral assemblage of this suite in the decreasing order of modal volume is plagioclase+orthopyroxene±quartz±alkali-feldspar+ilmenite±biotite. Biotites are seen to be in contact with orthopyroxene in most cases (Fig3b), but a few euhedral biotites are also prevalent. Structural studies previously undertaken have suggested that S1 schistosity associated with the earliest deformation is preserved in this unit and is subparallel to the compositional layering between the unit and the metapelites (Dobmeier and Raith, 2000).

3.2 *Garnetiferous Charnockites (G-Ch)*

Rock unit characterized by its coarse grained greasy appearance and garnetiferous nature (Fig 2e and f). It is significantly less voluminous than the EP and is seen to range in dimensions from small centimetre scale lenses and pods to metre scale bands and is predominant in the Hatia and Calcutta quarries although one small outcrop was observed in the Greenlake Quarry. Petrographically, it is quite similar to the leptynites in the region except for the presence of orthopyroxenes and coarser-grained nature. Myrmekites are ubiquitous and is seen to occur at the contact between alkali feldspar and plagioclase feldspar (Fig 3h). The mineral assemblage of this unit in decreasing order of modal volume is alkali feldspar+quartz+plagioclase+garnet+orthopyroxene+biotite+ilmenite (Fig 4a). Accessory minerals include zircon, apatite and monazite. Orthopyroxene is mostly seen to be in contact with garnet and biotite (Fig 3f) and is present in lesser modal proportion when compared to the EPs. Foliation associated with the earliest deformational event has been tentatively suggested for this unit (Bhattacharya et al., 1994) but the most pervasive foliation seen in the field is S2 (ENE-WSW) which has clearly overprinted any previous imprints. Microphotographs of sections perpendicular to the foliation plane reveal lenticular quartz, alkali-feldspar, plagioclase and the mafic minerals-orthopyroxene, biotite, garnet and ilmenite to be the foliation defining minerals (Fig 3g). K-feldspars exist as orthoclase.

3.3 *Non-Garnetiferous Charnockites (NG-Ch)*

Greasy green rock units that are coarse grained in nature and devoid of garnets (Fig 2b). These units are predominant in the northern quarries- USIS and Greenlake and are not prevalent in the quarries in the south. The unit also exhibits the pervasive foliation S2 (Fig 2b). This variant was also identified previously by (Bhattacharya et al., 1994) and was put under the broad umbrella of 'charnockitic rocks'. The mineral assemblage of this suite in the decreasing order of modal volume is alkali feldspar+quartz+plagioclase+orthopyroxene+ilmenite+biotite (Fig 4a). Petrographic studies show that most orthopyroxenes are in contact with biotite laths (Fig 3e). Sections prepared perpendicular to the foliation plane exhibits quartz, alkali-feldspar, plagioclase and mafic minerals-orthopyroxene, biotite and ilmenites as the foliation defining minerals while the ones prepared parallel to the foliation plane shows granoblastic texture with characteristic triple junctions (Fig 3d). Myrmekites are ubiquitous in this suite as well and K-feldspars exist as both orthoclase and microcline.

4. Analytical methods

For this study, a total of nine carefully selected samples (five EPs, two G-Ch and two NG-Ch) were processed for whole rock major and trace element analyses. The samples were cautiously collected from the central portions of the exposed lithological bands to avoid contamination from adjacent units. The major oxide data was generated using Bruker S8 Tiger sequential Wavelength Dispersive X ray Fluorescence Spectrometer (WD-XRF) at NCESS, Thiruvananthapuram. Pressed pellets were prepared using 40 mm aluminium cups filled with Boric acid crystals as binder. Finely powdered sample (-300 mesh) was sprinkled over boric acid (about 2g sample+ 8g boric acid) in the aluminium cup and was pressed in a hydraulic press with 30 ton pressure to produce a circular 40 mm disk. To estimate the accuracy of the readings, USGS rock standards BHVO-2 and G-2 pellets were run as unknowns. Total iron was measured as Fe_2O_3. The accuracy for the major elements were better than 5 %, and P_2O_5 showed accuracy range between 5-7 %. The trace element data including REEs were measured using the quadrupole Inductively Coupled Plasma Mass Spectrometer (ICPMS, Thermo Scientific X-Series II) at Centre for Earth Sciences, Indian Institute of Science, Bengaluru. The digestion and dilution procedure in (Banerjee et al., 2016) was followed for sample solution preparation. USGS international rock standards BHVO-2, AGV-2, BCR-2 and BIR-1a were run along with the samples to keep a check on accuracy. The accuracy for most elements was better than 5% and for the REEs, it was better than 3%. Internal precision based on three repeat measurements was between 2 to 3 % for all elements.

For mineral chemistry analyses, four representative thin sections of the orthopyroxene-bearing rock units (two EPs, one G-Ch and one NG-Ch) were processed for the chemical data of orthopyroxene, biotite, garnet, plagioclase and ilmenite. The concentrations were determined using JEOL JXA-8230 Electron Microprobe (EPMA) at the Advanced Facility for Microscopy and Microanalysis (AFMM) of the Indian Institute of Science, Bengaluru. The acceleration voltage was 15 kV, the probe current was 12 nA, and the probe diameter was set to 3 microns. The calibration was made using natural and synthetic silicates as well as oxides. The data corrections were made by following the standard ZAF correction procedures (Heinrich, 1991).

5. Results

5.1 Whole rock Geochemistry

5.1a Major and minor elements

The major and minor element chemistry of the orthopyroxene-bearing suites are given in Table 1 and has been illustrated through the plots given in Fig 4. The TAS diagram (Le Bas et al., 1986) shows the mafic to slightly intermediate nature of the EPs (with one isolated sample plotting on the ultramafic region) and felsic nature of the G-Ch and NG-Ch rocks (Fig 4b). The EPs shows metaluminous character in the A/CNK vs A/NK plot (Shand,1943) with A/NK values ranging from 3.60 to 7.75 while the G-Ch and NG-Ch rocks show slightly metaluminous character with A/NK values ranging from 1.59 to 1.61 and 1.40 to 1.42 respectively (Fig 4c). The AFM diagram (Irvine and Baragar, 1971) reveals the tholeiitic affinity of the EPs and the calc-alkaline affinities of the G-Ch and NG-Ch rocks (Fig 4d). The $FeO_t/(FeO_t+MgO)$ wt% vs SiO_2 wt% diagram (Frost and Frost, 2008) shows that the EPs exhibit magnesian to ferroan character while the G-Ch rocks show ferroan and NG-Ch rocks, slightly magnesian character (Fig 4f). When plotted on the Na_2O+K_2O-CaO wt% vs SiO_2 wt% diagram (Frost et al., 2001), the EPs straddle between the calcic and calc-alkalic fields while the G-Ch and NG-Ch samples plot on the calc-alkalic and alkali-calcic fields respectively (Fig 4g). In the normative Ab-An-Or diagram (Barker,1979), the EPs plot very close to An vertex while the G-Ch and NG-Ch rocks plot in the granite region (Fig 4h). As seen in Table 1, overall the high TiO_2, Al_2O_3, CaO, MgO, Fe_2O_3 and low SiO_2 and K_2O of the EPs are in sharp contrast with the composition ranges of these oxides for the G-Ch and NG-Ch rocks. The slightly higher CaO and lower Na_2O contents of the G-Ch rocks compared to the NG-Ch rocks are also notable.

5.1b Trace elements

The trace element data of orthopyroxene-bearing units is reported in Table 2. EPs exhibit lower and more variable Rb and Ba concentrations when compared to G-Ch rocks and NG-Ch rocks. The Sr concentrations in EPs range narrowly (103.58-113.20 ppm), with one outlier at 296.20 ppm, while G-Ch rocks show similar levels (111.50-172.30 ppm) and NG-Ch rocks exhibit significantly higher values (326.85-340.60 ppm). EPs exhibit Nb and Y concentrations in the range 8.60-33.23 ppm and 28.11-66.90 ppm respectively while G-Ch rocks show narrower ranges ([18.82-19.70 ppm] and [42.84-43.08 ppm]). Notably, NG-Ch rocks have low concentrations of Nb and Y (6.75-10.80 ppm and 6.60-8.16 ppm respectively). Zr abundance of the EPs are in the range 115-229 ppm. In comparison, the G-Ch rocks show a higher Zr abundance (163-224 ppm) while the NG-Ch samples, although high, exhibits a larger variation (26-254ppm).

In the chondrite normalized diagram, the EPs show a flat to slightly enriched LREE pattern [$(La/Sm)_n$=1.30-2.13], with no discernible HREE depletion [$(Gd/Yb)_n$ = 1.40-2.16]. The $(La/Yb)_n$ values range from 2.19-5.47 indicating a slightly fractionated REE pattern. An isolated sample shows a slightly positive Eu anomaly (1.14). The G-Ch rocks exhibit slightly higher LREE values [$(La/Sm)_n$=2.89-3.65], slightly higher HREE depletion [$(Gd/Yb)_n$=2.29-2.87] and a more fractionated overall REE pattern [$(La/Yb)_n$=9.10-11.05]. They also show a negative to slightly positive Eu/Eu* [0.64-1.08]. The REE pattern of the NG-Ch rocks diverge markedly from the EPs and G-Ch rocks as it shows high LREE enrichment [$(La/Sm)_n$=4.90-8.94], significant HREE depletion [$(Gd/Yb)_n$=5.76-11.67], and therefore a highly fractionated REE pattern [$(La/Yb)_n$=26.46-80.46] and variable Eu anomaly [Eu/Eu*=0.85-1.55] (Fig 5a and b)

In the primitive mantle normalized multi-element diagram, the EPs show high variability in the Rb values (around 10 times to more than 100 times the primitive mantle values) while the Ba values show a comparatively narrower range. There is no notable Nb anomaly and the values are around 10 times the primitive mantle values. A slightly positive K anomaly is observed for three samples (around 100 times the PM value) and a negative Sr anomaly is present, except for one sample. The lack of any notable Ti or Y anomalies is also conspicuous in the diagram. On the other hand, the G-Ch and NG-Ch rocks show more elevated Rb and Ba values. The presence of negative Ti anomaly and strong positive K anomaly is also evident in both rock units. One NG-Ch sample shows a negative Th anomaly. A negative Zr anomaly for one NG-Ch sample is also evident in the spider plot. The G-Ch rocks show a negative Sr anomaly while the NG-Ch rocks show flat to slightly positive Sr anomaly. Other notable contrasting feature includes the presence of a negative Y, Nb anomaly in the NG-Ch rocks. (Fig 6a and b)

5.2 Mineral Chemistry

Representative mineral chemistry data of orthopyroxenes and biotites from each unit are provided in Table 3. Orthopyroxenes in EPs range from ~En_{51} to ~En_{40}. They also have higher TiO_2 (~0.1-0.2%) and CaO (~0.8%) but lower Al_2O_3 (~0.7-0.8%) compared to other units. In contrast, orthopyroxenes in the G-Ch are ~En_{34} and exhibit lower TiO_2 (~0.1%) and CaO (~0.5%) but higher Al_2O_3 (~1.3%). Orthopyroxenes in NG-Ch are ~En_{40} and show similar X_{Mg} to those found in one variant of EP but have higher Al_2O_3 (~1.0%) and lower CaO (~0.5%) and TiO_2 (<0.1%), distinguishing them from EP orthopyroxenes. Biotites in EPs have high X_{Mg} (~0.70) relative to those in G-Ch (~0.41) while biotites in NG-Ch have intermediate X_{Mg} (~0.55). TiO_2 contents are high in biotites from both EP (4.5%) and G-Ch (5.7-5.9%), while NG-Ch biotites contain slightly lower TiO_2 (3.8-4.0%). Feldspar compositions are listed in Table 4. EP plagioclase is highly calcic, with An content ranging from ~An_{82} to ~An_{66}. Plagioclase in NG-Ch and G-Ch is more sodic but distinct in composition (~An_{32} and ~An_{52}, respectively). Garnet and opaque (oxides) compositions are shown in Table 5. Garnets in G-Ch are predominantly Almandine (~$Alm_{70}Pyr_{13}Grs_{15}Sps_2$). Opaques across all orthopyroxene-bearing units are ilmenites, with FeO_t of ~48% in EP, ~52% in NG-Ch, and ~50% in G-Ch.

6. Discussion

The major, trace, and mineral chemistry data clearly indicate that the three orthopyroxene-bearing units are distinct entities and cannot be grouped under the same umbrella. Their characteristics suggest that each unit may have originated from independent sources, so the nature of the source regions must be evaluated using robust proxies.

6.1 Element mobility

Since all the rock units have undergone significant metamorphism, it is crucial to examine the mobility of elements under these settings. The mobility of LILEs under such settings have been well documented, but the REEs and other HFSEs are generally regarded to be largely unaffected by metamorphic fluid activity (Bau, 1991). The plots shown in Fig 7 a through c can be used to examine the mobility of elements. The K/Rb vs K(wt%) plot (Rudnick and Presper,1990) shows that the G-Ch , NG-Ch rocks plot in the field of common igneous and sedimentary rocks with a higher K_2O value, while EG appears perturbed (Fig 7a). The Rb vs Sr (log-log) plot also shows that the overall trend of EG is incoherent (Fig 7b). The Th/U vs La/Th plot is an effective way to examine the depletion of U and Th (Rudnick and Presper, 1990). It shows that only a NG-Ch sample plots on the U loss side (Fig 7c). Overall, the trend of the REEs and other HFSEs composition within each orthopyroxene bearing unit (Fig 5, Fig 6) suggests that they are robust and can be used to comment on the characteristics of their precursors. The HREE+Y depletion observed in the NG-Ch rocks can be considered intrinsic to their precursor lithologies because if it were the activity of metamorphic fluids, it would have been prevalent in other units in the terrane as well, but this depletion is exclusive to the NG-Ch rocks. The coherent trend observed in Sr abundances within each unit suggests that it could also be used to make some broad conclusions about the true nature of the unit. The higher Sr contents of the NG-Ch rocks when compared to the other two rock units would therefore be reflective of the characteristics of their precursor lithologies. Overall, it is the case that only the EP elements appear to be incoherent, thus these variations could be intrinsic to the precursor.

6.2 Key insights from mineral chemistry

The mineral chemistry data reaffirm the distinctness of each orthopyroxene-bearing unit, as established by the bulk rock data (Fig 8). Petrographic associations suggest that the orthopyroxenes are likely of metamorphic origin, with compositional variations possibly linked to the nature of the reactant ferromagnesian minerals. In the EPs and NG-Ch rocks, the close association between biotite and orthopyroxene indicates that biotite is the main ferromagnesian phase dehydrating to form orthopyroxene (Fig. 8c and d). This potentially explains the higher modal volume of orthopyroxenes in the EPs as it could be a reflection of the initially high modal volume of biotite in the unit. The scarcity of biotite in one EP sample may therefore reflect its near-complete consumption (Fig 3c). In contrast, the G-Ch rocks show a close association between garnet, biotite, and orthopyroxene, suggesting that both biotite and garnet are involved in orthopyroxene formation (Fig. 8e). Although distinguishing metamorphic from igneous orthopyroxenes petrographically can be challenging in high-grade rocks (Touret & Huizenga, 2012), mineral chemistry provides a broader basis for distinction. Rajesh and Santosh (2011) compared X_{Mg} (molar Mg/(Mg+Fe)) and X_{Al} (=Al/2, where Al is the cation proportion for six oxygens) in orthopyroxenes from metamorphic zones and unmetamorphosed igneous charnockites. Their diagram showed that orthopyroxenes of igneous origin tend to exhibit lower and narrower X_{Al} values than those from metamorphic zones. Although they did not recommend the plot as a strict discrimination tool, it can still be used for broad classification, keeping in mind that it does not account for bulk rock compositional variations, as the reference dataset included only charnockites (sensu stricto). X_{Mg} and X_{Al} values of orthopyroxenes from the present study are plotted on the diagram adapted from (Meshram et al., 2021) (Fig. 8b). G-Ch orthopyroxenes fall within the dehydration field, EG orthopyroxenes plot mainly within the igneous field, and NG-Ch orthopyroxenes straddle both fields. However, as mentioned before, this diagram alone cannot be used to reach a conclusion regarding the EP orthopyroxenes as the plot does not appear to be useful in informing us about the composition range of orthopyroxenes in mafic-intermediate units. In this context, it is necessary to consider the composition of the reactant phases involved while interpreting the origin of orthopyroxenes. The higher X_{Mg} and lower X_{Al} in EP orthopyroxenes likely reflect the the higher X_{Mg} of associated biotites, which are compositionally phlogopitic (Fig. 9a). Their lower X_{Al} content also corresponds with the lower Al content of the reactant biotite (Table 3). Similarly, within the G-Ch rocks, garnets in contact with orthopyroxene show lower X_{Mg} (~0.15) compared to other G-Ch garnets (X_{Mg} ~0.17), supporting garnet breakdown during orthopyroxene formation. When it comes to the plagioclases, the ones found in EPs are clearly distinct from those in NG-Ch and G-Ch rocks. The higher An content (~82) is highly unlike the composition observed in regular granitoids. (Fig 9b). The plagioclase compositions of the G-Ch and NG-Ch shows that the range is within what is generally observed in granitoids and their differences also point to the distinctness of the units.

6.3 Implications of geochemistry for tectonic setting

Since tectonic discrimination diagrams employing mobile elements may not reliably represent the rock units in this study, they were excluded. Although the Ta vs Yb plot (Pearce et al., 1984) shows that all rock units plot largely within the volcanic arc field, only the NG-Ch rocks can be confidently categorized as exhibiting a proper VAG like signature (Fig 7f). As Sr abundances are coherent, as discussed in section 6.1, the Sr/Y vs Y diagram (Martin, 1986; Hansen et al., 2002; Defant and Drummond, 1990) was used, showing that the NG-Ch rocks plot fairly within the adakite field, with Sr/Y values ranging between 41 and 47 (Fig 7e). Given that the study area is a complex terrane, the actual scenario is likely more nuanced than what is suggested solely by discrimination diagrams, as inputs from multiple sources and partial melting events of various source units, depending on their fertility and heat sources, may occur in orogenic belts. The geochemical data appears to be in-line with potential processes in a convergent tectonic environment. However, whether they are more indicative of an accretionary or collisional setting requires further evaluation through more detailed studies and comparison with rock suites from well-studied regions. These aspects are undertaken and further discussed in section 6.3.

6.3 Original nature of precursors

6.3a EP

Although enderbitic units are generally interpreted to represent metamorphosed tonalites, this rock suite appears to be different and not fit that line of interpretation. The bulk rock compositions are mostly mafic, with composition of plagioclase ranging from An_{82} to An_{66}, which is not the range generally expected if it is a tonalite (sensu stricto) (Le Maitre, 1976, 2002). Although the modal proportions of quartz is equal to or slightly above 20% in selected samples, most of the varieties do not possess the characteristic modal volume observed in tonalites, with some even plotting in the diorite/gabbro/anorthosite region (Fig 4a). Previous studies attributed this to igneous grading, but the variations in the modal volume and bulk rock compositions suggest that an alternative process might be the reason behind this nature of the unit. As the normative feldspar diagram reveals (Fig 4h), the samples are not plotting in the tonalite region but instead very close to the anorthite vertex. This is reflective of the highly calcic composition of the plagioclases. Interestingly, a recent study (Bose et al., 2020) has argued for the presence of a metagreywacke unit in the field, and after the comparison of field images and photomicrographs, it is clear that the OFGs they present and the EPs discussed in this study are the same entities. Clearly, a depositional origin can better explain the trends observed in the bulk rock chemistry. Under this interpretation of the unit, the variations in the Eu/Eu*(0.39-1.14) can be suggestive of a multi-component provenance, and based on such signatures along with extremely high An composition observed in non-migmatitic variants of EP and the overall high modal volume of such grains, this study speculates the presence of mafic components in the provenance for the unit, along with the felsic components already suggested based on the study of detrital zircons from this unit (Bose et al., 2020). Another interesting implication of this interpretation is that the ultramafic xenoliths previously suggested to be within this unit are possibly lithic fragments of an ultramafic component in the provenance. This essentially suggests a short transport distance and mineralogical immaturity, suggesting rapid erosion of nearby mafic-ultramafic sources. This is in alignment with the interpretation that the unit likely represents arc-derived turbidity sequences (Bose et al., 2020) Overall the bulk rock and mineral chemistry data are more in-line with the conclusions drawn regarding the metagreywacke unit in the region (Bose et al., 2020) and it highlights the complexity of the depositional history of the terrane. A detailed provenance study of this unit can provide much insights on the earliest history of the Chilka lake area.

6.3b G-Ch

The overall homogeneity in the chemical composition of the G-Ch rocks is very conspicuous in the trace element diagrams (section 5.1b, Fig 6b) which suggests minimal fractionation. Although the G-Ch suite differs from the leptynites in macroscopic appearance, the two are remarkably similar petrographically, with the presence of orthopyroxene in the former being the only distinguishing feature under thin section. The HFSE data of the G-Ch rocks also appear to be highly similar to the leptynites (Fig 10). The average composition of Post-Archean Indian shale (Ray and Paul, 2021) is also plotted for reference. Since it is established that the precursors to the leptynites arose via the mica dehydration melting of the previously existing metapelitic suite in the region (Sen&Bhattacharya, 1997), this study is compelled to test the validity of such a mode of petrogenesis for the G-Ch rocks. Interestingly, although the CaO (3.3-3.7 wt%), Fe_2O_3t (3.7-4.2 wt%), MgO(0.57-0.69wt%) abundances of G-Ch rocks is slightly higher than what is usually observed in leptynites, the true range of the compositions of leptynites (CaO = 0.63-3.29wt%; Fe_2O_3t = 0.9-5.5wt%; MgO = 0.15-3.00wt%)(Sen and Bhattacharya 1997) reveal that G-Ch like compositions are present within the meta-leucogranitoid unit. According to the dehydration melting modelling previously attempted on the metapelite-leptynite system, a few samples were categorized as signs of disequilibrium, namely samples such as L-10, L-13, and L-15 belonging to the H-cluster of compositional range, as they exhibited overall higher Fe, Ca, and Mg along with notable variations in Y, Zr, Nb, and Ti than what is usually observed in leptynites (Sen and Bhattacharya, 1997). They suggested that this is best explained by restite entrainment, with the observed variations controlled by the mineralogy of the entrained restite. Interestingly, the composition range of such samples is comparable to the G-Ch rocks, as they also exhibit similar variations in the abundances of the aforementioned elements (Table 1,2). When compared to a leptynite that is more or less representative of an equilibrium melt, the elevated abundances of Nb and Ti in G-Ch rocks are clearly noticeable in the spider plot (Fig 10). In addition to that, the higher Eu and Sr concentrations also reinforce the 'restite entrainment' interpretation. (Fig 10, Table 2) In the light of such a possibility, this study postulates that the G-Ch rocks are most likely disequilibrium melts derived from the prevalent metapelitic suite, with restite entrainment being a probable cause of the disequilibrium.

The field evidence is in fact indicative of the proposed origin of G-Ch rocks, because they were always observed away from the metapelitic suite within the study region and was never seen to be in contact with it, a pattern similar to the field relations exhibited by the leptynites, suggestive of melt migration (Fig 1b). The low voluminous nature of G-Ch could also possibly be explained in the light of the suggested restite entrainment, because then it is possible that the G-Ch rocks are likely representative of melts in the waning stage of the dehydration melting event, after the peak volume stage, which is represented by the leucogranitoids. Finally, the presence of orthopyroxene (only small modal volume) in only the G-Ch and not the leptynites is therefore likely reflective of the bulk composition, and as previously discussed, the orthopyroxene formed by reaction involving both garnet and biotite.

Furthermore, the similar isotopic signatures of the khondalites (metapelitic suite), charnockites, and leptynites in the region (Rickers et al., 2001) support the interpretation that the both these granitoids are genetically linked to the prevalent metapelitic suite.

6.3c NG-Ch

The NG-Ch rocks as previously discussed is a distinct entity characterized by its highly fractionated REE pattern, low Nb, Ti, Y and higher Sr concentration. Based on the volume of the unit as observed in the field, and the absence of any mafic-intermediate unit with a similar geochemical signature in the area, the NG-Ch precursors are more likely representative of products of partial melting rather than products of fractionation. Coming to a possible source region, the most likely explanation, in light of the current understanding of the geodynamic history of the region, appears to be melting of a crustal source which already possess the aforementioned geochemical signatures. As the HREE+Y depletion is suggestive of residual garnet, melting of older lower crustal TTG gneisses (possibly formed in an arc setting during a past event) which can generate sufficient volume of melt to eventually rise and emplace into the upper crustal metasedimentary suite appears to be a plausible model. This way, the negative Nb, Ti anomaly, high $(La/Yb)_n$ and high Sr/Y ratios could be explained as signatures directly inherited from the source region.

However, fluid absent melting experiments on sodic TTGs suggest that the resulting melts are usually low in K_2O (Watkins et al., 2007), thereby indicating that significant volumes of high K_2O granites cannot be explained as melt products of TTGs. Interestingly, taking into consideration this ‘low K_2O’ problem, a granite suite identified in the Fiskenæsset region having a ‘TTG’ like signature just like the NG-Ch was interpreted to be a product of partial melting of predominantly granodioritic component of a lower crustal TTG, thereby explaining its higher K_2O abundances ((Huang et al., 2016). This interpretation was further corroborated by the presence of negative Eu anomalies in representative granites. The compositional range of the Fiskenæsset region granites (excluding altered samples and cumulates) is shown in Fig 11. Interestingly, the NG-Ch rocks exhibit a similar trend, but with notable differences in the Eu anomalies and degree of HREE depletion. Although the current dataset of NG-Ch rocks is limited, the trends in the Eu anomaly and ΣREE are suggestive of melt evolution, with the sample with the least ΣREE (~70ppm) showing a positive Eu anomaly (~1.55) and a more evolved sample (ΣREE= ~285ppm) showing a slightly negative Eu anomaly (~0.85). A comparison of the composition range of Fiskenæsset region granites with the trend of the NG-Ch suite suggests that the latter is likely more enriched in incompatible elements overall. This, by extension, reflects a slightly more enriched source for the NG-Ch. However, irrespective of these nuances in the nature of source TTG, the fractionated pattern is common to both, and the signature anomalies in the spider plots also align, implying a similar mode of petrogenesis. In light of these aspects, this study suggests that the NG-Ch rocks were likely formed via dehydration melting of a lower crustal TTG gneiss, with melts derived predominantly from the granodioritic component. Though the NG-Ch rocks are voluminous enough to be mappable, they are not of batholith scale, therefore such a mode of petrogenesis appears consistent. Regarding the mechanism that could have triggered this melting, crustal thickening associated with the peak of the orogenic event in the region (D2) appears to be the most plausible. The presence of this entity, therefore, signifies the complex crustal anatexis history of the Chilka lake area.

6.4 Evolution of terrane

Based on the obtained understanding of the origin of the orthopyroxene-bearing entities in the field, it is important to properly place them in the timescale of the evolution of the Chilka lake area. If we go by the argued similar deformational histories of the metagreywackes and metapelites, then it seems to be the case that both these sedimentary units were likely established before the first deformation event (D1), thereby making them the oldest entities in the region. On the basis of EPMA dating of monazites from khondalites, the timing of the D1 event has been estimated to be between 1250 and 1100 Ma (Simmat and Raith, 2008). The leucogranitoids are interpreted to have been formed during the foliation-defining and crustal anatexis phase (D2), which is identified to have occurred between 980 and 940 Ma (Simmat and Raith, 2008), thereby making them a later addition. If the proposed mode of origin of G-Ch precursors is correct, they also formed during the same time-frame. As the origin of NG-Ch rock precursors also appears to involve crustal anatexis, it is likely that they also formed during the D2 stage, as they too possess the pervasive S2 foliation. The precursors to mafic granulites and anorthosites identified further south of the Chilka lake area are potentially linked to Rodinia breakup (Bose et al., 2011b; Chakrabarti et al., 2011), which suggests that they are likely younger than the aforementioned entities. This study therefore highlights that crustal reworking was the dominant process during the Rodinia assembly, with notable juvenile additions occurring only later, during Rodinia breakup.

7. Conclusions

- The geochemical study of orthopyroxene-bearing entities in the northern Chilka Lake area suggests that each identified unit, i.e., EPs, G-Ch, and NG-Ch, represents a distinct lithology originating from an independent source.

- The field aspects, bulk rock and mineral chemistry data of the EPs are more consistent with a depositional origin, with a provenance likely involving, felsic, mafic and minor ultramafic rocks, thereby reaffirming their previous characterization as akin to arc derived turbidity sequences.
- The G-Ch rocks are likely products of disequilibrium melting of the prevalent metapelitic suite in the region, with the cause of disequilibrium likely being restite entrainment.
- NG-Ch rocks are likely products of partial melting of predominantly granodioritic component of a lower crustal TTG, with their characteristic signature likely inherited from the source region.
- This study emphasizes the intricate depositional history and complex crustal anatexis events of the Chilka lake area. It also highlights the overall complexity of granulite terranes, which can alter the original nature of rock units to such an extent that their present characteristics may at times be misleading.

8. Future Prospects

Although the newly identified charnockites are likely linked to crustal reworking during the peak phase of Grenvillian orogeny, high-resolution geochronological studies of the units are necessary to better constrain the timing of their origin. Moreover, isotopic proxies can be used to further assess the validity of the modes of petrogenesis proposed in this study. It appears to be the case that the metagreywacke unit and the NG-Ch were not included in previous comprehensive isotopic studies of Domain 3 (Rickers et al., 2001). The provenance studies of the greywacke unit will also shed light on the true nature of the source of sediments, therefore readers with expertise in that domain are encouraged to take up such research.

Acknowledgements

A part of this work was carried out by the author as master's research. The author would like to thank Dr. Yengkhom Kesorjit Singh, Indian Institute of Technology, Bhubaneswar for providing a supportive research environment. The author is grateful to Prof. Ramananda Chakrabarti, Indian Institute of Science, Bengaluru, for the support provided during the trace element analyses and for helpful suggestions. The author gratefully acknowledges insightful discussions with Dr. Christoph Dobmeier and Prof. Michael Raith, which were beneficial to this study. The author extends his gratitude to Dr. Chiranjeeb Chatterjee, EPMA lab, Indian Institute of Science, Bengaluru for all the help provided in obtaining the mineral chemistry data. The help from Mrs. Lakshmi, XRF lab, National Centre for Earth Science Studies, Trivandrum, for the major oxide data acquisition is also acknowledged. The author would also like to thank Mr. Sourav Kumar Naik for all the help provided during fieldwork.

References

Banerjee, A., Chakrabarti, R., & Mandal, S. 2016. Geochemical anatomy of a spheroidally weathered diabase. *Chemical Geology*, **440**, 124–138.

Barker, F. 1979. Trondhjemite: Definition, environment and hypotheses of origin. In *Developments in Petrology* **6**, 1–12

Bau, M. 1991, Rare-earth element mobility during hydrothermal and metamorphic fluid-rock interaction and the significance of the oxidation state of europium *Chemical Geology,* **93** 219-230

Bhattacharya, S. Sen, S. K., and Acharyya, A., 1993 Structural evidence supporting a remnant origin of patchy charnockites in the Chilka Lake area, India; *Geol. Mag.* **130** 363-368

Bhattacharya, S. Sen, S. K., and Acharyya, A., 1994 Structural setting of the Chilka Lake granulite migmatite-anorthosite suite with emphasis on the time relation of charnockites; *Precambrian Res.* **66** 393-409

Bhattacharya, S. 1996 Eastern Ghats granulite terrain of India: An overview; *J. Southeast Asian Earth Science.* **14** 165-174

Bhattacharya, S., Kar R, Misra S and Teixeira W 2001 Early Archaean Continental crust in the Eastern Ghats granulite belt, India: Isotopic evidence from a charnockite suite; *Geol. Mag.* **138** 609-618

Bhattacharya, S., Chaudhary, A. K., & Basei, M. 2012. Original nature and source of khondalites in the Eastern Ghats Province, India. *Geological Society Special Publication*, **365**(1), 147–159.

Bose, S., Das, K., Torimoto, J., Arima, M., & Dunkley, D. J. 2016. Evolution of the Chilka Lake granulite complex, northern Eastern Ghats Belt, India: First evidence of ~ 780 Ma decompression of the deep crust and its implication on the India–Antarctica correlation. *Lithos*, **263**, 161–189.

Bose, S., Das, K., Torimoto, J., & Dunkley, D. 2020. Origin of orthopyroxene-bearing felsic gneiss from the perspective of ultrahigh-temperature metamorphism: an example from the Chilka Lake migmatite complex, Eastern Ghats Belt, India. *Mineralogical Magazine*, **84**(5), 712–737.

Bose, S., Das, K., Chakraborty, S., Miura, H., 2011b. Petrology and geochemistry of metamorphosed basic intrusives from Chilka Lake granulites, Eastern Ghats Belt, India: implications for Rodinia breakup. In: Srivastava, R.K. (Ed.), Dyke swarms: keys for geodynamic interpretation. Springer-Verlag, Heidelberg, 241–262.

Chakrabarti, R., Basu, A.R., Bandyopadhyay, P.K., and Zou, H., 2011, Age and origin of the Chilka anorthosites, Eastern Ghats, India:implications for massif anorthosite petrogenesis and break-up of Rodinia. In: Ray, J., Sen, G., and Ghosh, B. (Eds.), Topics in Igneous Petrology. Springer, Berlin, 355–382.

Collerson, K.D., Fryer, B.J. 1978 The role of fluids in the formation and subsequent development of early continental crust. *Contrib.Mineral. Petrol.* **67**, 151-167

Dasgupta, S., Bose, S., & Das, K. 2013. Tectonic evolution of the Eastern Ghats Belt, India. *Precambrian Research*, **227**, 247–258.

Das, K., Bose, S., Karmakar, S., Chakraborty, S., 2012. Petrotectonic framework of granulites from northern part of Chilka Lake area, Eastern Ghats Belt, India: compressional vis-`a-vis transpressional tectonics. *Journal of Earth System Sciences* **121**, 1–17.

Deer, W.A., Howie, R.A., & Zussman, J. 1992. An Introduction to the Rock-Forming Minerals (2nd ed.). Longman Scientific & Technical, Essex, 696 pp.

Defant, M.J ., Drummond, M.S, 1990 Derivation of some modern arc magmas by melting of young subducted lithosphere. *Nature*, **347**, 662–665

Dobmeier C and Raith M 2000 On the origin of 'arrested' charnockitization in the Chilka Lake area, Eastern Ghats Belt, India: a reappraisal; *Geol. Mag.* **137** 27-37

Dobmeier, C., Simmat, R., 2002. Post-Grenvillian transpression in the Chilka Lake area, Eastern Ghats Belt — implications for the geological evolution of peninsular India. *Precambrian Research* **113**, 243–268

Dobmeier, C.J., Raith, M.M., 2003. Crustal architecture and evolution of the Eastern Ghats Belt and adjacent regions of India. In: Yoshida, M., Windley, B.F., Dasgupta, S. (Eds.), Proterozoic East Gondwana: Supercontinent Assembly and Breakup. *Geological Society London Special Publication* **206**, 145–168.

Frost, B.R., Arculus, R.J., Barnes, C.G., Collins, W.J., Ellis, D.J., Frost, C.D., 2001. A geochemical classification of granitic rocks. Journal of Petrology **42**, 2033–2048.

Frost, B.R., Frost, C.D., 2008. On charnockites. *Gondwana Research* **13**, 30-44.

Green, T.H., Brunfelt, A.O., Heier, K.S. 1972 Rare-earth element distribution and K/Rb ratios in granulites, mangerites, and anorthosites, Lofoten-vesteraalen, Norway. *Geochim. Cosmochim. Acta* **36**, 241-257

Halden N M, Bowes D R and Dash B 1982 Structural evolution of migmatites in a granulite facies terrane: Precambrian crystalline complex of Angul, Orissa, India; *R. Soc. Edinburgh* **73** 109-118

Hamilton, P.J., Evensen, N.M., O'Nions, R.K., Tarney, J. 1979 Sm- Nd systematics of Lewisian gneisses: Implications for the origin of granulites. *Nature* **277**, 25-28

Hansen, J., Skjerlie, K. P., Pedersen, R. B., & de La Rosa, J. 2002. Crustal melting in the lower parts of island acrs: An example from the Bremanger Granitoid Complex, West Norwegian Caledonides. *Contributions to Mineralogy and Petrology*, **143**(3), 316–335.

Harlow E.D 2012 The potential role of fluids during regional granulite facies dehydration in the lower crust. *Geoscience Frontiers* **3**(6) 813-827

Heinrich, K.F.J., Newbury, D., 1991. Electron Probe Quantitation, First ed. New York.

Huang, H., Polat, A., & Fryer, B. J. 2013. Origin of Archean tonalite-trondhjemite-granodiorite (TTG) suites and granites in the Fiskenæsset region, southern West Greenland: Implications for continental growth. *Gondwana Research*, **23**(2), 452–470.

Irvine, T. N. & Baragar, W. R. A. 1971. A guide to the chemical classification of the common volcanic rocks. *Canadian Journal of Earth Sciences* **8,** 523–548.

Le Bas, M. J., Le Maitre, R. W., Streckeisen, A. & Zanettin, B. 1986. A chemical classification of volcanic rocks based on the total alkali–silica diagram. *Journal of Petrology* **27,** 745–750.

Le Maitre, R. W. 1976. The chemical variability of some common igneous rocks. *Journal of Petrology*, **17**(4), 589–598.

Le Maitre, R. W. (Ed.) 2002. Igneous rocks: A classification and glossary of terms (2nd ed.). Cambridge University Press

Martin, H., 1986 Effect of steeper Archean geothermal gradient on geochemistry of subduction-zone magmas *Geology* **1** (4), 753-756

McDonough, W.F., Sun, S.-S., 1995. The composition of the Earth. *Chemical Geology* **120**, 223-253.

McLennan, S.M. 1989 Rare Earth Elements in Sedimentary Rocks: Influence of Provenance and Sedimentary Process. *Review of Mineralogy*, 21, 169-200.

Meshram, T., Dora, M. L., Baswani, S. R., Upadhyay, D., Meshram, R., Randive, K., Ranjan, S., & Nanda, J. K. 2021. Petrogenesis and U- Pb geochronology of charnockites flanking the Pranhita Godavari rift in peninsular India-link between the Bastar and Eastern Dharwar Cratons. *Gondwana Research*, **92**, 113–132.

Miyashiro A. 1974. Volcanic rock series in island arcs and active continental margins. American *Journal of Science* **274**, 321–355.

Morimoto, N., Fabries, J., Ferguson, A.K., Ginzburg, I.V., Ross, M., Seifert, F.A. and Zussman, J. (1988) Nomenclature of Pyroxenes. *American Mineralogist*, 73, 1123-1133.

Pearce, Julian A., Nigel BW Harris, and Andrew G. Tindle. 1984 Trace element discrimination diagrams for the tectonic interpretation of granitic rocks. *Journal of petrology* **25** (4) 956-983.

Rajesh, H. M., Santosh, M., & Yoshikura, S. 2011. The Nagercoil charnockite: A magnesian, calcic to calc-alkalic granitoid dehydrated during a granulite-facies metamorphic event. *Journal of Petrology*, **52**(2), 375–400.

Ray E., Paul. D 2021 Major and Trace Element Characteristics of the Average Indian Post-Archean Shale: Implications for Provenance, Weathering, and Depositional Environment *ACS Earth and Space Chemistry* **5** (5), 1114-1129

Rickers, K., Mezger, K., Raith, M.M., 2001. Evolution of the continental crust in the Proterozoic Eastern Ghats Belt, and new constraints for Rodinia reconstruction: implications from Sm–Nd, Rb–Sr and Pb–Pb isotopes. *Precambrian Research* **112**, 183–212.

Rudnick, R.L., Presper, T., Vielzeuf, D., Vidal, P., 1990. Geochemistry of intermediate-to high-pressure granulites. In: Granulites and Crustal Evolution. Kluwer Academic Publishers, 523-550

Sarkar, T., Schenk, V., & Berndt, J. 2015. Formation and evolution of a Proterozoic magmatic arc: geochemical and geochronological constraints from meta-igneous rocks of the Ongole domain, Eastern Ghats Belt, India. *Contributions to Mineralogy and Petrology*, **169**(1), 1–27.

Sen, S.K., Bhattacharya, S., Acharyya, A., 1995. A multi-stage pressure–temperature record in the Chilka Lake granulites: the epitome of the metamorphic evolution of Eastern Ghats, India? *Journal of Metamorphic Geology* **14**, 287–298.

Sen S K and Bhattacharya S 1997 Dehydration melting of micas in the Chilka Lake khondalites: The link between the metapelites and granitoids; *Proc. Indian Acad. Sci. (Earth Planet. Sci.)* **106** 277-297

Shand, S. J. 1943. Eruptive Rocks. Their Genesis, Composition, Classification, and Their Relation to Ore-Deposits with a Chapter on Meteorite. New York: John Wiley & Sons.

Simmat, R., & Raith, M. M. 2008. U-Th-Pb monazite geochronometry of the Eastern Ghats Belt, India: Timing and spatial disposition of poly-metamorphism. *Precambrian Research*, **162**(1–2), 16–39.

Sun, S.-S., McDonough, W.F., 1989. Chemical and isotopic systematics of oceanic basalts: implications for mantle composition and processes. *Geological Society Special Publications* **42**, 313-345

Taylor, S. R. and McLennan, S. M. 1995: The geochemical evolution of the continental crust, *Review Geophysics*, **33**, 241–265

Touret, J.L.R., Huizenga, J.M., 2012. Charnockite microstructures: From magmatic to Metamorphic. *Geoscience Frontiers* **3**(6) 745-753

Watkins, J., Clemens, J., Treloar, P., 2007. Archaean TTGs as sources of younger granitic magmas: melting of sodic metatonalites at 0.6–1.2 GPa. *Contributions to Mineralogy and Petrology* **154**, 91–110.

Tables

Table 1: Major-oxide compositions of orthopyroxene-bearing entities and one leptynite

Sample	GRL02	CAL04	HAT04	CAL02	USIS02	HAT01	CAL01	USIS01	GRL03	HATLP
Rock Type	EP	EP	EP	EP	EP	G-Ch	G-Ch	NG-Ch	NG-Ch	Leptynite
Major oxides (wt%)										
SiO_2	42.70	49.44	51.36	52.48	51.42	66.54	68.66	67.29	68.03	71.01
TiO_2	1.96	1.31	1.50	1.35	2.41	0.72	0.63	0.35	0.48	0.35
Al_2O_3	19.86	17.37	17.29	15.83	17.63	15.20	14.69	14.47	15.28	14.13
Fe_2O_3(t)	15.27	11.90	11.83	12.19	13.42	4.21	3.77	4.88	3.28	2.65
MnO	0.16	0.16	0.15	0.14	0.19	0.05	0.05	0.04	0.04	0.04
MgO	5.81	6.38	5.06	5.95	2.77	0.69	0.57	1.45	0.85	0.21
CaO	11.67	9.83	8.32	7.87	8.06	3.66	3.26	2.7	2.62	2.69
Na_2O	1.11	1.61	1.65	1.24	1.92	1.60	1.98	2.53	2.65	2.08
K_2O	0.68	1.52	1.91	2.17	0.59	6.27	5.53	5.53	6.07	6.00
P_2O_5	0.31	0.17	0.38	0.31	0.84	0.35	0.31	0.25	0.18	0.30
Total	99.53	99.69	99.45	99.53	99.25	99.29	99.45	99.49	99.48	99.46
Mg#	43.00	51.53	45.89	49.18	29.04	24.52	23.06	37.07	33.94	13.59
K_2O/Na_2O	0.61	0.94	1.16	1.75	0.31	3.92	2.79	2.18	2.29	2.88

Mg# = molar Mg/(Mg+Fe^{2+})

Table 2: Trace element compositions of orthopyroxene-bearing entities and one leptynite

Sample	GRL02	CAL04	HAT04	CAL02	USIS02	HAT01	CAL01	USIS01	GRL03	HATLP
Rock Type	EG	EG	EG	EG	EG	G-Ch	G-Ch	NG-Ch	NG-Ch	Leptynite
Trace elements (ppm)										
Rb	3.86	72.15	12.58	134.70	4.23	219.20	275.60	167.10	163.30	202.70
Ba	84.38	118.60	58.47	238.30	66.78	1618.00	875.80	1280.00	1722.00	601.40
Sr	296.20	104.70	103.58	113.20	111.00	172.30	111.50	313.10	340.60	82.70
Pb	2.44	8.52	9.65	15.51	7.54	32.08	38.51	27.82	36.42	35.21
Th	0.55	0.09	0.14	4.07	1.15	4.36	6.52	0.26	26.08	3.88
U	0.13	0.05	0.17	1.86	0.28	0.28	0.46	0.29	0.68	0.32
Zr#	135	115	154	124	229	224	163	26	254	272
Ta	0.83	0.68	0.85	0.84	1.81	1.09	1.11	0.20	0.37	0.84
Y	28.11	38.42	40.47	41.41	66.90	42.84	43.08	6.60	8.15	40.28
Nb	9.65	8.60	15.32	11.61	33.23	19.70	18.82	6.76	10.80	13.39
Sc	36.13	38.73	36.25	39.38	44.55	8.29	5.84	4.88	2.80	8.40
Cr	80.30	301.70	254.00	216.10	85.48	13.54	10.91	187.50	14.42	5.39
Ni	72.02	47.63	35.77	34.84	39.32	11.56	11.22	67.41	9.63	3.29
Co	81.56	69.91	55.80	69.50	71.48	55.69	59.69	47.35	38.92	28.45
V	267.10	239.10	207.39	223.80	193.50	50.32	39.61	75.14	45.06	14.42
Zn	23.51	18.85	10.11	32.24	26.92	15.00	15.36	12.34	10.20	44.40
Cu	61.43	47.96	29.96	49.50	103.20	29.91	21.83	48.98	14.34	8.73
La	8.05	15.99	23.19	30.21	38.63	51.42	50.92	16.6	76.05	45.61
Ce	20.73	36.38	58.93	71.92	92.66	101.8	106.90	29.29	131.30	90.61
Pr	3.09	4.86	6.69	9.38	12.30	11.54	12.42	3.16	13.40	10.35
Nd	14.47	19.79	28.04	38.25	53.66	45.52	50.65	11.52	42.81	39.48
Sm	4.00	5.11	7.02	9.15	13.79	9.09	11.35	2.19	5.52	8.40
Eu	1.59	1.17	1.28	1.37	1.85	3.59	2.43	1.33	2.04	1.76
Gd	4.94	6.05	7.22	10.36	15.25	11.26	11.51	3.14	9.57	9.34
Tb	0.76	0.95	1.18	1.34	2.19	1.38	1.62	0.29	0.61	1.33
Dy	4.99	6.23	7.49	7.58	12.27	7.43	8.29	1.26	1.80	7.73
Ho	1.04	1.32	1.53	1.51	2.44	1.54	1.52	0.23	0.32	1.49
Er	2.87	3.74	4.30	4.14	6.61	4.29	3.55	0.56	0.80	4.01
Tm	0.43	0.58	0.63	0.62	0.96	0.61	0.50	0.07	0.10	0.57
Yb	2.64	3.59	3.91	3.96	6.15	4.05	3.30	0.45	0.68	3.53
Lu	0.38	0.51	0.58	0.57	0.88	0.57	0.46	0.06	0.10	0.51
ΣREE	69.53	106.31	152.01	190.37	259.65	254.09	265.44	70.15	285.10	224.72
Eu/Eu*	1.14	0.64	0.55	0.43	0.39	1.08	0.64	1.55	0.85	0.61
$(Gd/Yb)_{CN}$	1.41	1.39	1.52	2.16	2.05	2.30	2.88	5.76	11.67	2.19
$(La/Yb)_{CN}$	2.19	3.20	4.25	5.47	4.51	9.10	11.04	26.46	80.45	9.28

CN- Chondrite normalized, Eu/Eu*= $(Eu)_{CN}/[(Sm)_{CN} \times (Gd)_{CN}]^{0.5}$, #data from XRF

Table 3: Microprobe data and cation proportions of Orthopyroxene and Biotite

Sample	GRL02	USIS02	HAT01	GRL03	GRL02	HAT01	HAT01	GRL03	GRL03
Mineral	Opx	Opx	Opx	Opx	Bt	Bt	Bt	Bt	Bt
SiO_2	51.76	50.05	48.62	49.68	38.41	35.35	35.75	37.89	38.01
TiO_2	0.17	0.10	0.07	0.07	4.54	5.91	5.71	3.80	3.98
Al_2O_3	0.79	0.74	1.30	1.03	12.37	13.06	13.08	13.56	13.60
Cr_2O_3	0.00	0.00	0.06	0.02	0.17	0.07	0.04	0.05	0.00
FeO_t	28.88	34.33	38.11	34.73	12.63	22.60	22.73	18.01	18.14
MnO	0.49	0.82	0.37	0.50	0.01	0.02	0.04	0.04	0.00
MgO	17.39	13.32	11.54	13.48	16.36	8.75	8.64	12.60	12.99
CaO	0.77	0.80	0.50	0.52	0.01	0.05	0.00	0.04	0.04
Na_2O	0.03	0.07	0.00	0.05	0.06	0.00	0.00	0.09	0.10
K_2O	0.00	0.00	0.00	0.00	10.35	9.66	9.99	10.15	10.12
F	0.00	0.00	0.00	0.01	3.16	0.92	1.12	-	-
Cl	0.01	0.02	0.01	0.01	0.25	0.07	0.07	-	-
H_2O_{calc}	-	-	-	-	2.59	3.43	3.36	3.98	4.01
O=F+Cl	-	-	-	-	-1.39	-0.41	-0.49	-	-
Total	100.29	100.25	100.59	100.09	99.52	99.48	100.04	100.19	100.99
O basis	6	6	6	6	22	22	22	22	22
Si	1.98	1.98	1.95	1.97	5.55	5.46	5.49	5.71	5.68
Ti	0.00	0.00	0.00	0.00	0.49	0.69	0.66	0.43	0.48
Al	0.04	0.03	0.06	0.05	2.10	2.38	2.37	2.41	2.40
Cr	0.00	0.00	0.00	0.00	0.02	0.01	0.01	0.01	0.00
Fe^{2+}	0.93	1.14	1.28	1.15	1.53	2.92	2.92	2.27	2.27
Mn	0.02	0.03	0.01	0.02	0.00	0.00	0.01	0.01	0.00
Mg	0.99	0.79	0.69	0.80	3.52	2.02	1.98	2.83	2.90
Ca	0.03	0.03	0.02	0.02	0.00	0.01	0.00	0.01	0.01
Na	0.00	0.01	0.00	0.00	0.02	0.00	0.00	0.03	0.03
K	0.00	0.00	0.00	0.00	1.91	1.90	1.96	1.95	1.93
F	0.00	0.00	0.00	0.00	1.44	0.45	0.54	-	-
Cl	0.00	0.00	0.00	0.00	0.06	0.02	0.02	-	-
OH	-	-	-	-	2.50	3.53	3.44	4.00	4.00
X_{Mg}	0.52	0.41	0.35	0.41	0.70	0.41	0.40	0.55	0.56

XMg = Mg/(Mg+Fe^{2+}), calc- H_2O contents of Bt calculated by stoichiometry

Table 4: Microprobe data and cation proportions of feldspars

Sample	GRL02	GRL02	USIS02	USIS02	GRL03	GRL03	HAT01	HAT01
Mineral	Pl(core)	Pl(rim)	Pl(core)	Pl(rim)	Pl(core)	Pl(rim)	Pl(core)	Pl(rim)
SiO_2	48.00	47.96	51.45	51.32	60.27	60.33	54.17	53.27
TiO_2	0.00	0.00	0.03	0.04	0.02	0.04	0.00	0.00
Al_2O_3	33.28	33.64	30.80	31.02	24.68	24.88	28.74	29.33
Cr_2O_3	0.00	0.00	0.00	0.01	0.00	0.01	0.00	0.03
FeO_t	0.10	0.19	0.16	0.21	0.08	0.19	0.05	0.15
MnO	0.00	0.04	0.00	0.02	0.00	0.00	0.00	0.00
MgO	0.00	0.02	0.01	0.00	0.00	0.00	0.00	0.00
CaO	16.69	16.76	13.93	13.98	6.92	6.88	11.04	12.01
Na_2O	2.04	2.14	3.69	3.53	7.90	7.82	5.44	4.81
K_2O	0.04	0.05	0.18	0.14	0.24	0.20	0.24	0.21
Total	100.15	100.81	100.25	100.28	100.11	100.34	99.68	99.83
O basis	8	8	8	8	8	8	8	8
Si	2.20	2.18	2.34	2.33	2.69	2.68	2.46	2.42
Ti	0.00	0.00	0.00	0.00	0.00	0.00	0.00	0.00
Al	1.79	1.81	1.65	1.66	1.30	1.30	1.54	1.57
Cr	0.00	0.00	0.00	0.00	0.00	0.00	0.00	0.00
Fe^{2+}	0.00	0.01	0.01	0.01	0.00	0.01	0.00	0.01
Mn	0.00	0.00	0.00	0.00	0.00	0.00	0.00	0.00
Mg	0.00	0.00	0.00	0.00	0.00	0.00	0.00	0.00
Ca	0.82	0.82	0.68	0.68	0.33	0.33	0.54	0.58
Na	0.18	0.19	0.32	0.31	0.68	0.67	0.48	0.42
K	0.00	0.00	0.01	0.01	0.01	0.01	0.01	0.01
An	81.70	81.00	66.91	68.08	32.17	32.34	52.14	57.31
Ab	18.07	18.70	32.07	31.11	66.47	66.53	46.50	41.51
Or	0.23	0.30	1.01	0.81	1.35	1.13	1.36	1.18

Table 5: Microprobe data and cation proportions of Garnet and Ilmenite

Sample	HAT01	HAT01	GRL02	USIS02	GRL03	HAT01
Mineral	Grt	Grt	Ilm	Ilm	Ilm	Ilm
SiO_2	37.65	37.73	0.00	0.00	0.00	0.00
TiO_2	0.00	0.03	52.67	50.50	47.50	50.14
Al_2O_3	20.69	20.92	0.03	0.02	0.02	0.01
Cr_2O_3	0.00	0.00	0.20	0.09	0.12	0.04
FeO_t	32.19	32.08	47.07	48.58	52.19	50.07
MnO	0.87	0.85	0.49	0.49	0.25	0.20
MgO	3.16	3.64	0.25	0.44	0.21	0.24
CaO	5.35	5.23	0.00	0.00	0.00	0.00
Na_2O	0.00	0.00	0.04	0.02	0.03	0.00
K_2O	0.00	0.00	0.01	0.00	0.00	0.00
Total	99.92	100.48	100.74	100.14	100.31	100.73
O basis	12	12	3	3	3	3
Si	3.01	3.00	0.00	0.00	0.00	0.00
Ti	0.00	0.00	0.99	0.97	0.93	0.96
Al	1.95	1.96	0.00	0.00	0.00	0.00
Cr	0.00	0.00	0.00	0.00	0.00	0.00
Fe^{2+}	2.15	2.13	0.99	1.03	1.13	1.07
Mn	0.06	0.06	0.01	0.01	0.01	0.00
Mg	0.38	0.43	0.01	0.02	0.01	0.01
Ca	0.46	0.44	0.00	0.00	0.00	0.00
Na	0.00	0.00	0.00	0.00	0.00	0.00
K	0.00	0.00	0.00	0.00	0.00	0.00
Alm	70.49	69.61	-	-	-	-
Pyr	12.46	14.05	-	-	-	-
Grs	15.08	14.38	-	-	-	-
Sps	1.97	1.96	-	-	-	-

Figure Captions

Fig 1: Simplified Geological map of the study region. (a) Modified after Geological and Mineral Map of Orissa (2011) - Geological Survey of India. (b) Lithological map of the studied stone quarries showing sample locations.

Fig 2: Field images from the study area (a) Folded EP layer within metatexite metapelite. (b) Non-garnetiferous charnockite with prominent S2 foliation. (c) Dismembered blocks of EPs within the lepytnite. (d) A close-up of EP and leptynite. (e) Garnetiferous charnockite with prominent S2 foliation. (f) Garnetiferous charnockite displaying pervasive S2 foliation, as observed in the southernmost quarry.

Fig 3: Photomicrographs of orthopyroxene-bearing units. (a) Representative photomicrograph of EP exhibiting the characteristic granoblastic texture. (b) Biotite in contact with orthopyroxene in EP. (c) Orthopyroxene and ilmenite in EP with a paucity in biotite. (d) Representative photomicrograph of non-garnetiferous charnockite showing the typical granoblastic texture. (e) Orthopyroxene in contact with biotite and ilmenite in the non garnetiferous charnockite. (f) Orthopyroxene in contact with garnet, ilmenite, and biotite in the garnetiferous charnockite. (g) Elongate orthopyroxene in contact with garnet, defining the S2 foliation in garnetiferous charnockite. (h) Close-up of the ubiquitous myrmekitic texture along the boundary between alkali and plagioclase feldspars in garnetiferous charnockite. Mineral abbreviations follow IMA conventions

Fig 4: Classification diagram for orthopyroxene bearing units (a) QAP plot (After Frost and Frost, 2008) (b) TAS diagram (After Le Bas et al. 1986) (c) A/CNK [$Al_2O3/(CaO+Na_2O+K_2O)$] vs. A/NK [$Al_2O_3/(Na_2O+K_2O)$] diagram (After Shand, 1943) (d) AFM diagram (After Irvine&Baragar, 1971) (e) FeO_t/MgO vs SiO_2 discrimination diagram (After Miyashiro, 1974) (f) $FeO_t/(FeO_t+MgO)$ wt% vs SiO_2 (After Frost and Frost,2008) (g) Na_2O+K_2O-CaO (MALI) vs. SiO_2 diagram (Frost et al., 2001) (h) Normative feldspar diagram (After Barker 1979). Legend same as Fig 1b

Fig 5: Chondrite normalized REE plots for (a) EP, (b) G-Ch and NG-Ch. Normalization values from (Sun and McDonough, 1989). Average composition of UCC from (Taylor and McLennan, 1995) and PAAS from (McLennan, 1989)

Fig 6: Primitive mantle normalized diagram for (a) EP, (b) G-Ch and NG-Ch. Normalization values from (Sun and McDonough, 1989). Average composition of UCC from (Taylor and Mclennan, 1995)

Fig 7: Geochemical plots to assess element mobility and plausible tectonic setting (a) K/Rb vs K(wt%) (Rudnick and Presper, 1990) (b) Rb vs Sr. UCC and mantle values from (Taylor and McLennan, 1995) and (Sun and McDonough, 1989) respectively. Th/U vs La/Th (Rudnick and Presper, 1990) (d) Eu/Eu* vs ΣREE (e) Sr/Y vs Y (Martin, 1986; Hansen et al., 2002; Defant and Drummond, 1990) (f) Ta vs Yb (Pearce et al., 1984) See main text for discussion.

Fig 8: Classification diagrams and BSE images of orthopyroxenes (a) Ternary classification diagram (Wo-En-Fs) (Morimoto et al., 1988) (b)XAl vs XMg plot (Rajesh and Santosh, 2011) (Meshram et al., 2021). See main text for discussion. (c)Biotite in contact with orthopyroxene in EP. (d)Biotite within orthopyroxene in NG-Ch. (e) Orthopyroxene in contact with both garnet and biotite in G-Ch. Mineral abbreviations follow IMA conventions

Fig 9: Classification diagrams for biotite and feldspars (a) Biotite classification plot using Al^{IV} vs Fe/ (Fe + Mg) (Deer et al., 1992). (b) Ternary classification diagram Ab-An-Or for feldspars

Fig 10: Spider plot comparing the G-Ch rocks with leptynite; the average composition of Post-Archean Indian Shale (Ray and Paul, 2021) is also plotted for reference. See main text for discussion.

Fig 11: Spider plot comparing the NG-Ch unit with the composition range of Fiskenæsset region granites (Huang et al., 2016) (excluding altered samples and cumulates). See main text for discussion.

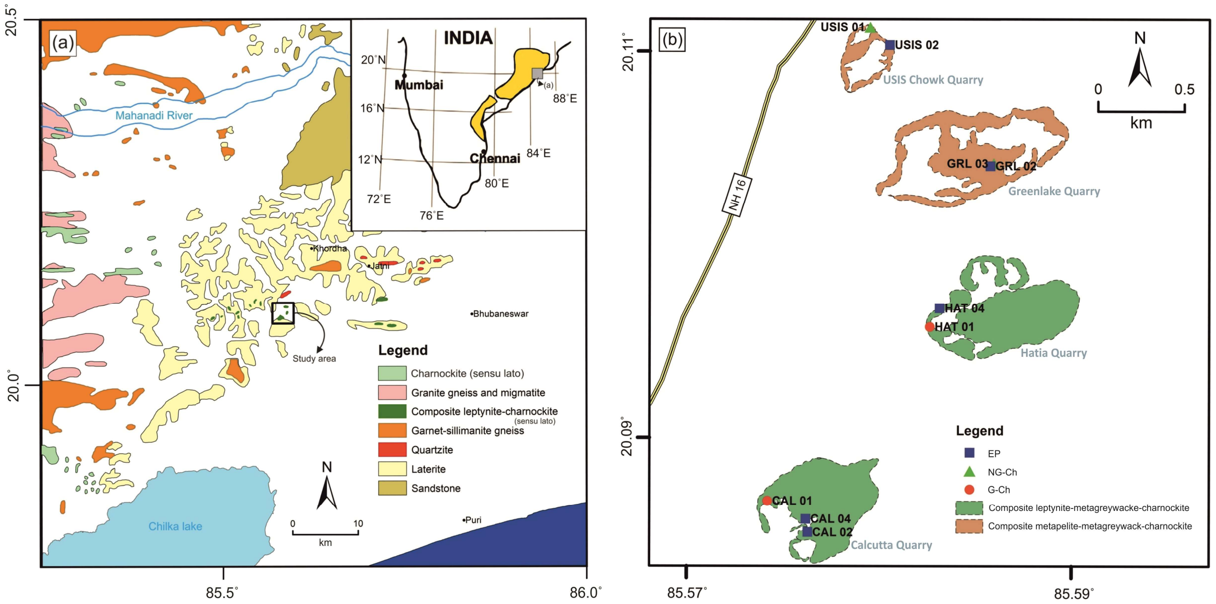
(a)
20.5˚
20.0˚
85.5˚
86.0˚
INDIA
20˚N
16˚N
12˚N
72˚E
76˚E
80˚E
84˚E
88˚E
Mumbai
Chennai
(a)
Mahanadi River
Khordha
Jatni
Bhubaneswar
Study area
Chilka lake
Puri
N
0
10
km
Legend
Charnockite (sensu lato)
Granite gneiss and migmatite
Composite leptynite-charnockite (sensu lato)
Garnet-sillimanite gneiss
Quartzite
Laterite
Sandstone
(b)
20.11˚
20.09˚
85.57˚
85.59˚
NH 16
USIS 01
USIS 02
USIS Chowk Quarry
GRL 03
GRL 02
Greenlake Quarry
HAT 04
HAT 01
Hatia Quarry
CAL 01
CAL 04
CAL 02
Calcutta Quarry
N
0
0.5
km
Legend
EP
NG-Ch
G-Ch
Composite leptynite-metagreywacke-charnockite
Composite metapelite-metagreywack-charnockite

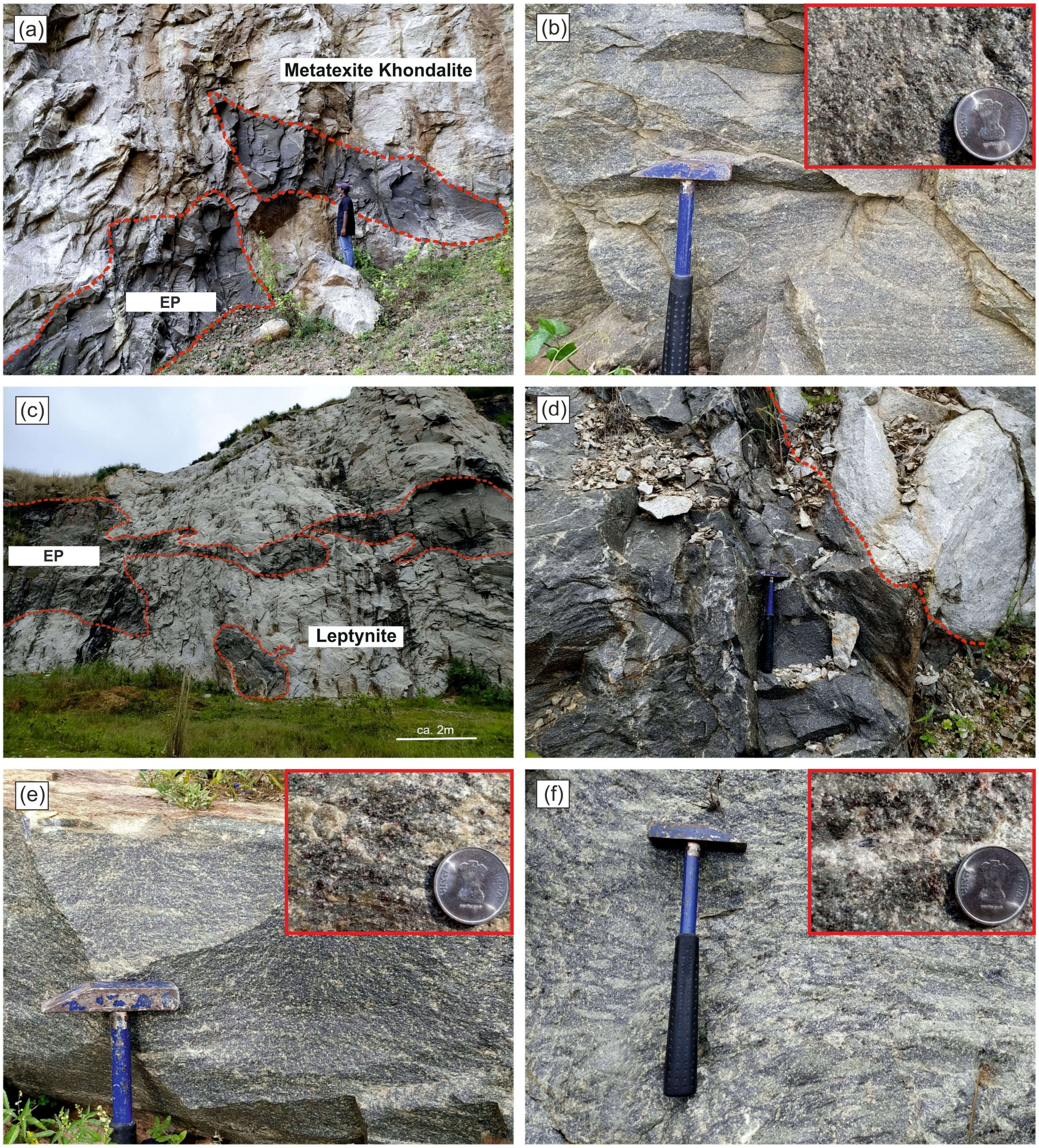
(a)
Metatexite Khondalite
EP
(b)
(c)
EP
Leptynite
ca. 2m
(d)
(e)
(f)

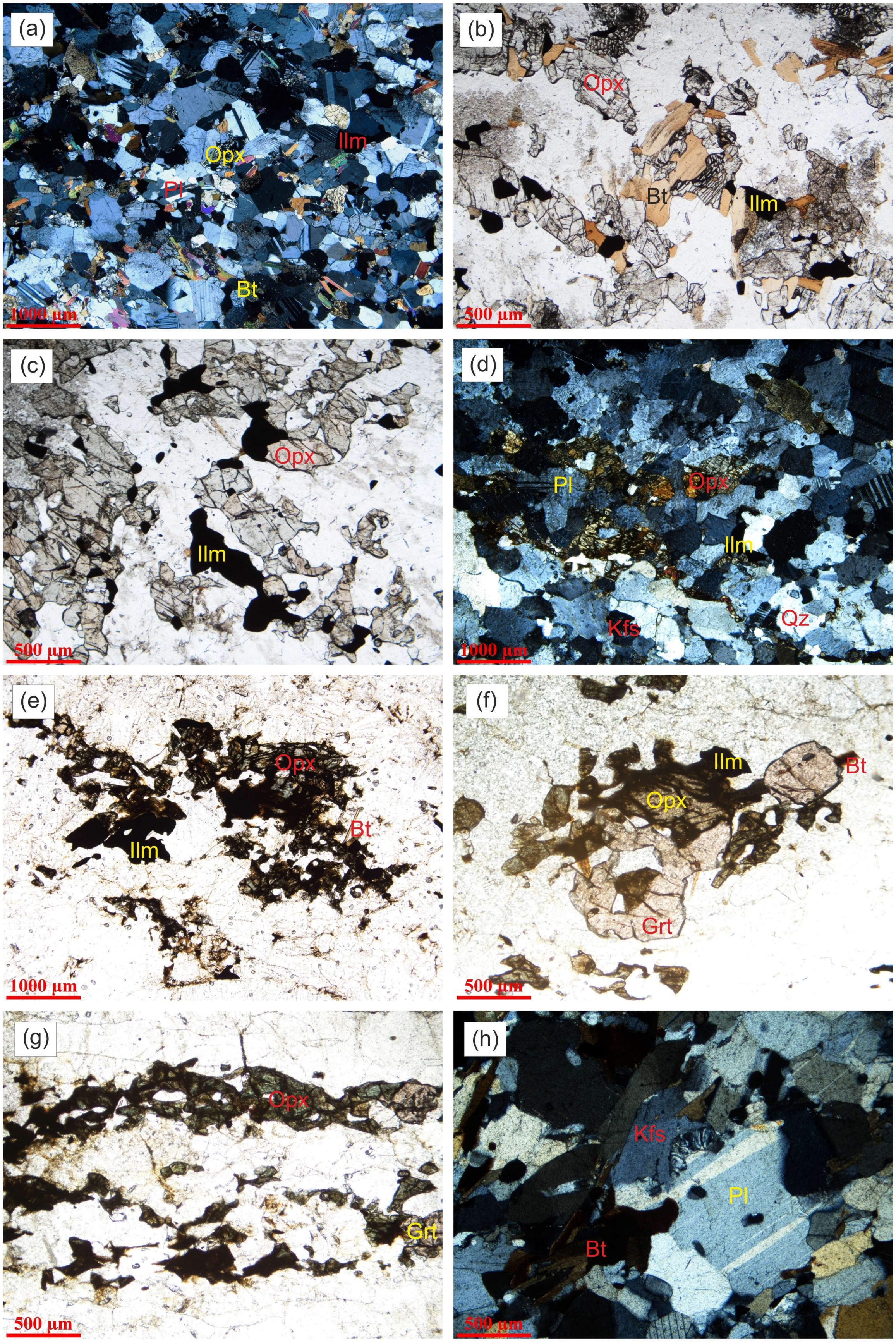
(a)
Ilm
Opx
Pl
Bt
1000 µm
(b)
Opx
Bt
Ilm
500 µm
(c)
Opx
Ilm
500 µm
(d)
Pl
Opx
Ilm
Kfs
Qz
1000 µm
(e)
Opx
Bt
Ilm
1000 µm
(f)
Ilm
Bt
Opx
Grt
500 µm
(g)
Opx
Grt
500 µm
(h)
Kfs
Pl
Bt
500 µm

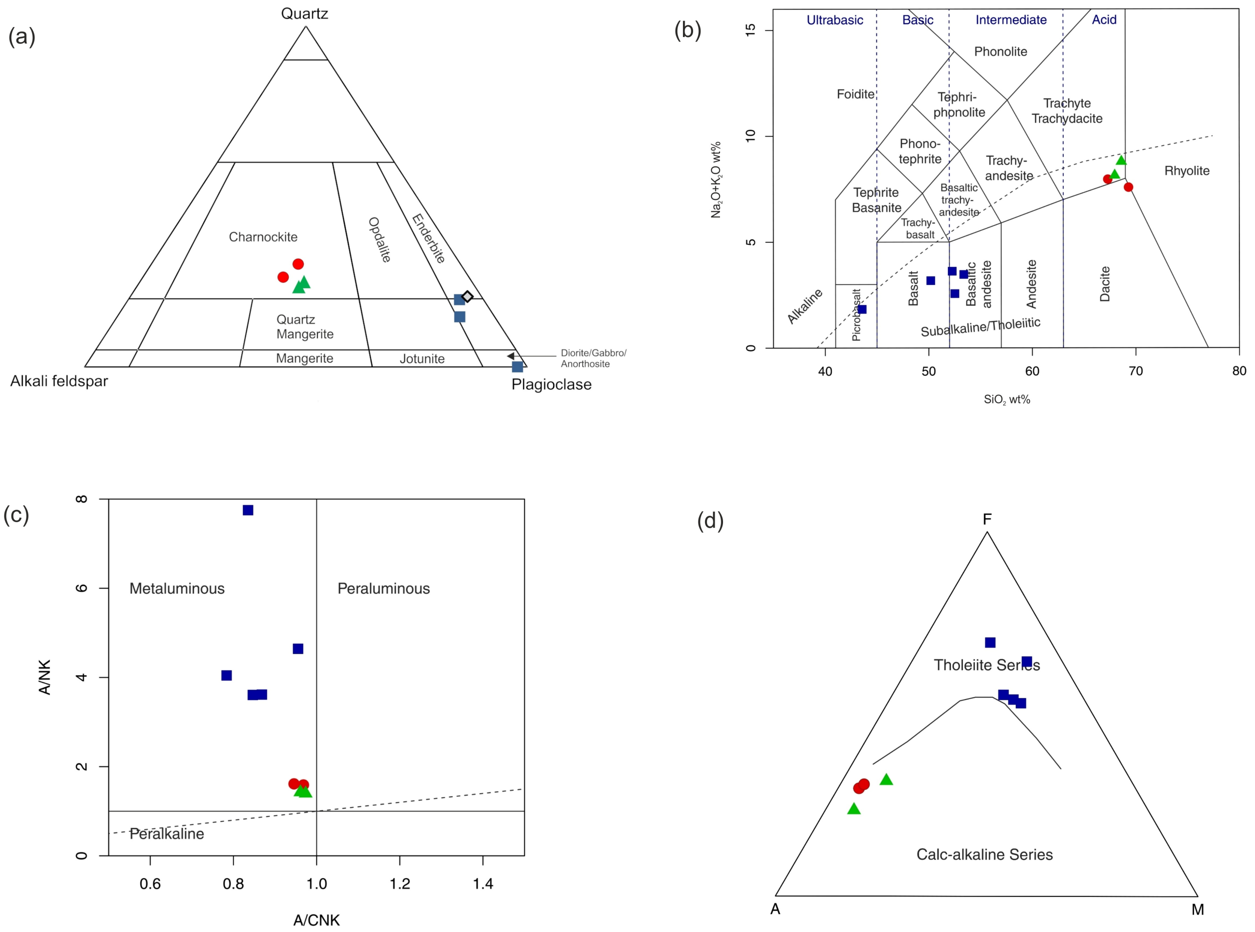
(a)
Quartz
Charnockite
Opdalite
Enderbite
Quartz Mangerite
Mangerite
Jotunite
Diorite/Gabbro/ Anorthosite
Alkali feldspar
Plagioclase
(b)
Ultrabasic
Basic
Intermediate
Acid
Phonolite
Foidite
Tephri-phonolite
Trachyte Trachydacite
Phono-tephrite
Trachy-andesite
Rhyolite
Tephrite Basanite
Basaltic trachy-andesite
Trachy-basalt
Alkaline
Picrobasalt
Basalt
Basaltic andesite
Andesite
Dacite
Subalkaline/Tholeiitic
Na_2O+K_2O wt%
SiO_2 wt%
0
5
10
15
40
50
60
70
80
(c)
Metaluminous
Peraluminous
Peralkaline
A/NK
A/CNK
0
2
4
6
8
0.6
0.8
1.0
1.2
1.4
(d)
F
Tholeiite Series
Calc-alkaline Series
A
M

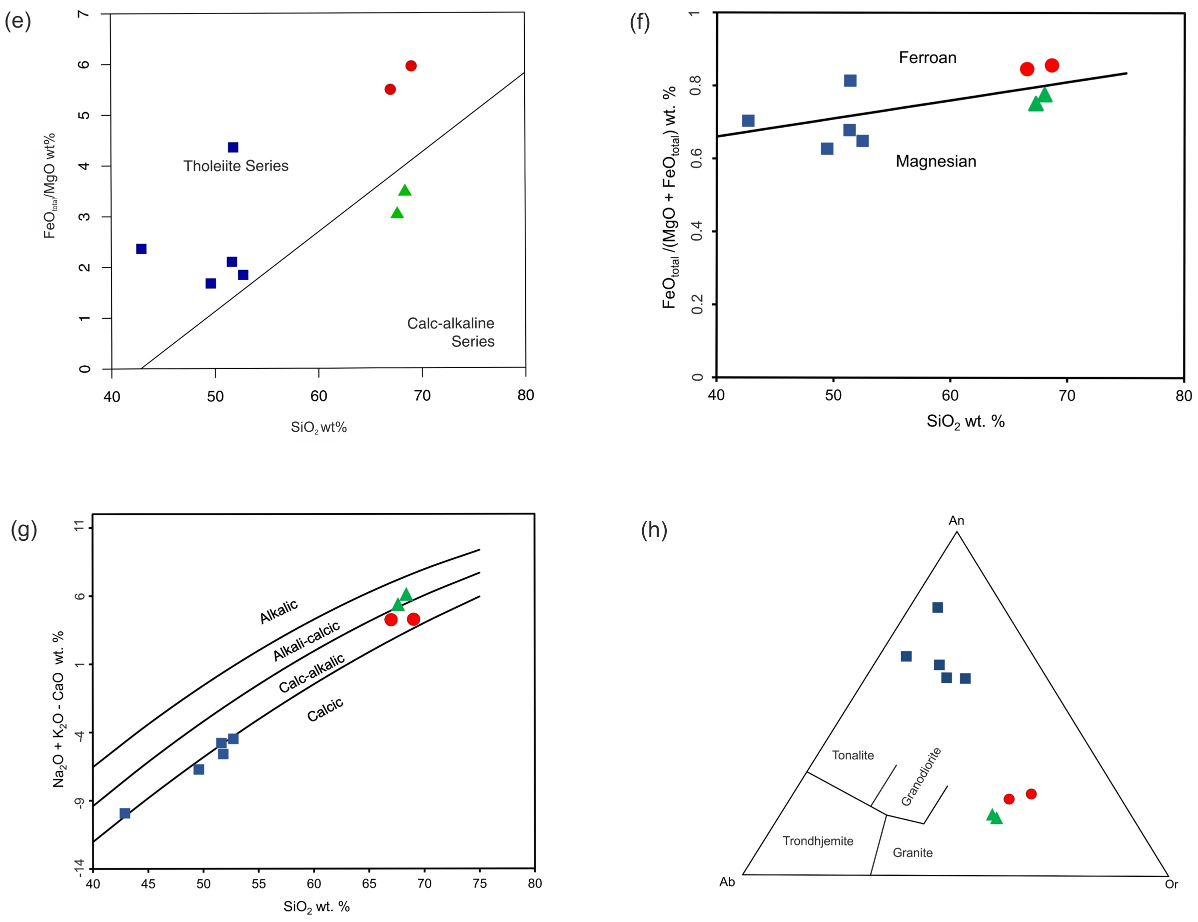
(e)
FeO_{total}/MgO wt%
SiO$_2$ wt%
Tholeiite Series
Calc-alkaline Series
0
1
2
3
4
5
6
7
40
50
60
70
80
(f)
$FeO_{total}/(MgO + FeO_{total})$ wt. %
SiO$_2$ wt. %
Ferroan
Magnesian
0
0.2
0.4
0.6
0.8
1
40
50
60
70
80
(g)
$Na_2O + K_2O - CaO$ wt. %
SiO$_2$ wt. %
Alkalic
Alkali-calcic
Calc-alkalic
Calcic
-14
-9
-4
1
6
11
40
45
50
55
60
65
70
75
80
(h)
An
Ab
Or
Tonalite
Granodiorite
Trondhjemite
Granite

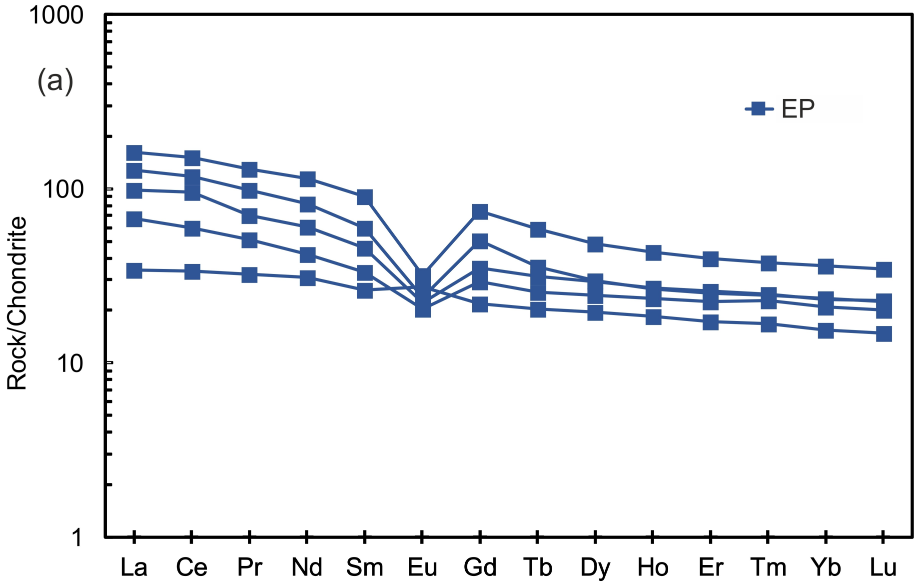
(a)
EP
Rock/Chondrite
1000
100
10
1
La
Ce
Pr
Nd
Sm
Eu
Gd
Tb
Dy
Ho
Er
Tm
Yb
Lu

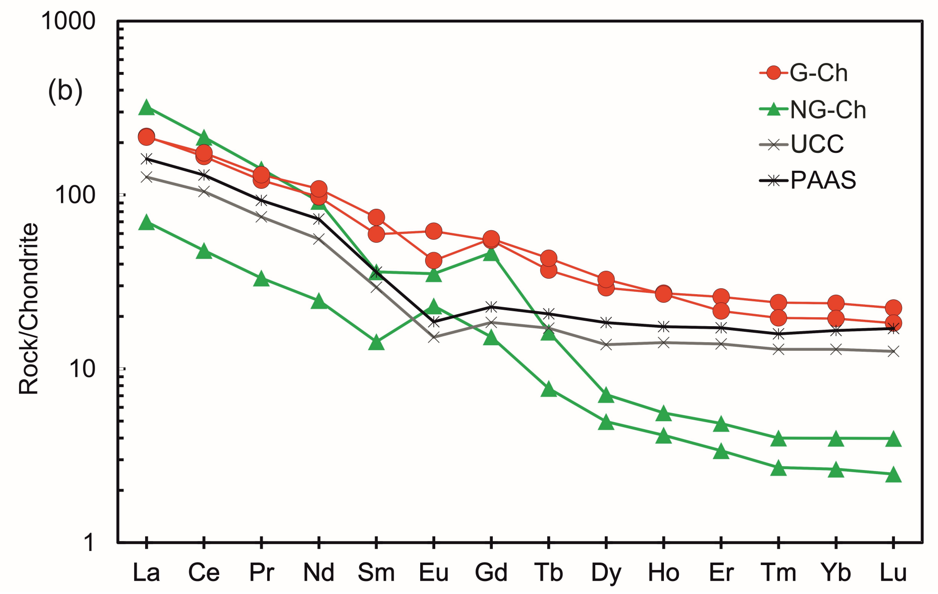
(b)
G-Ch
NG-Ch
UCC
PAAS
Rock/Chondrite
1000
100
10
1
La
Ce
Pr
Nd
Sm
Eu
Gd
Tb
Dy
Ho
Er
Tm
Yb
Lu

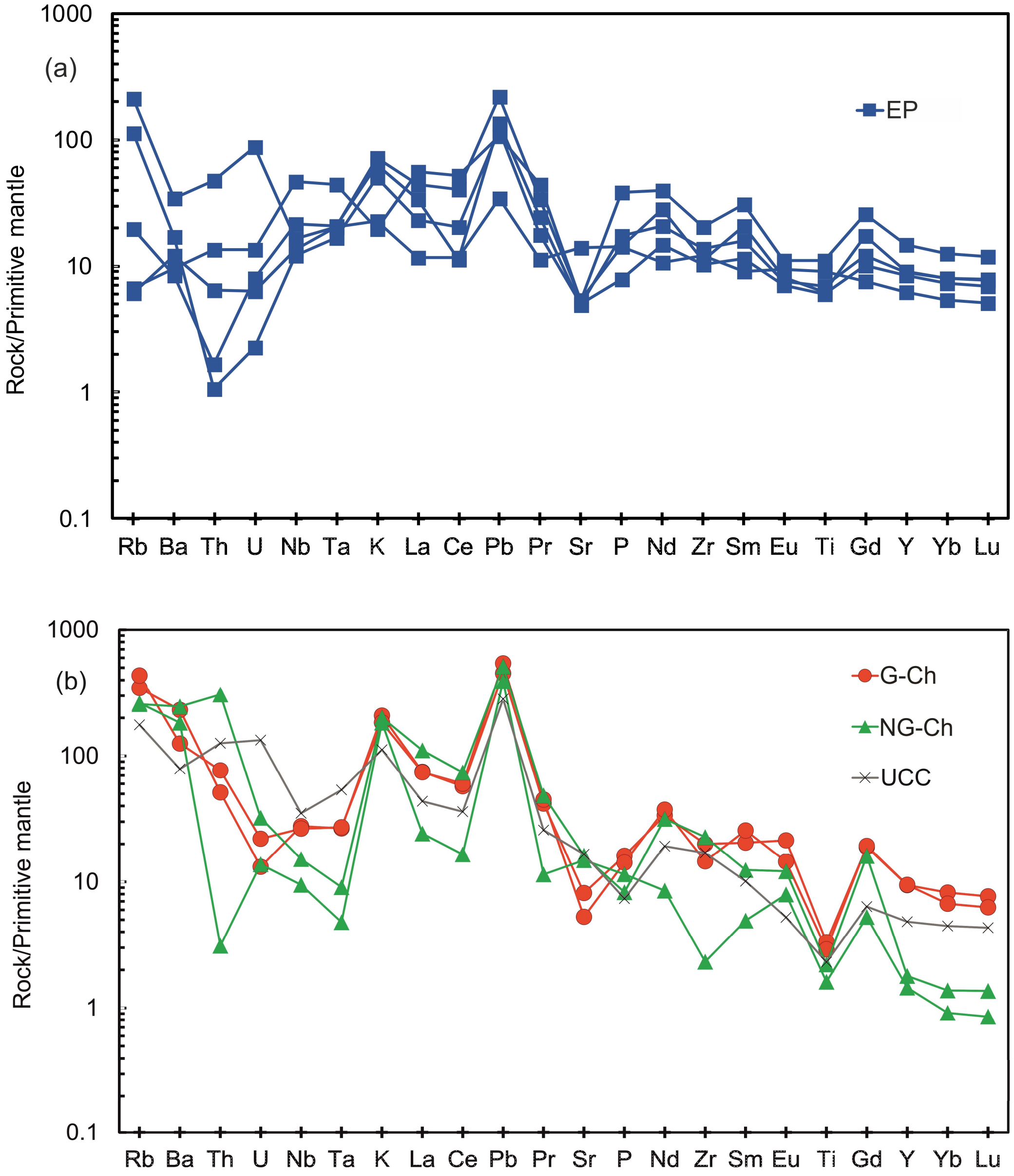
(a)
1000
100
10
1
0.1
Rock/Primitive mantle
EP
Rb Ba Th U Nb Ta K La Ce Pb Pr Sr P Nd Zr Sm Eu Ti Gd Y Yb Lu
(b)
1000
100
10
1
0.1
Rock/Primitive mantle
G-Ch
NG-Ch
UCC
Rb Ba Th U Nb Ta K La Ce Pb Pr Sr P Nd Zr Sm Eu Ti Gd Y Yb Lu

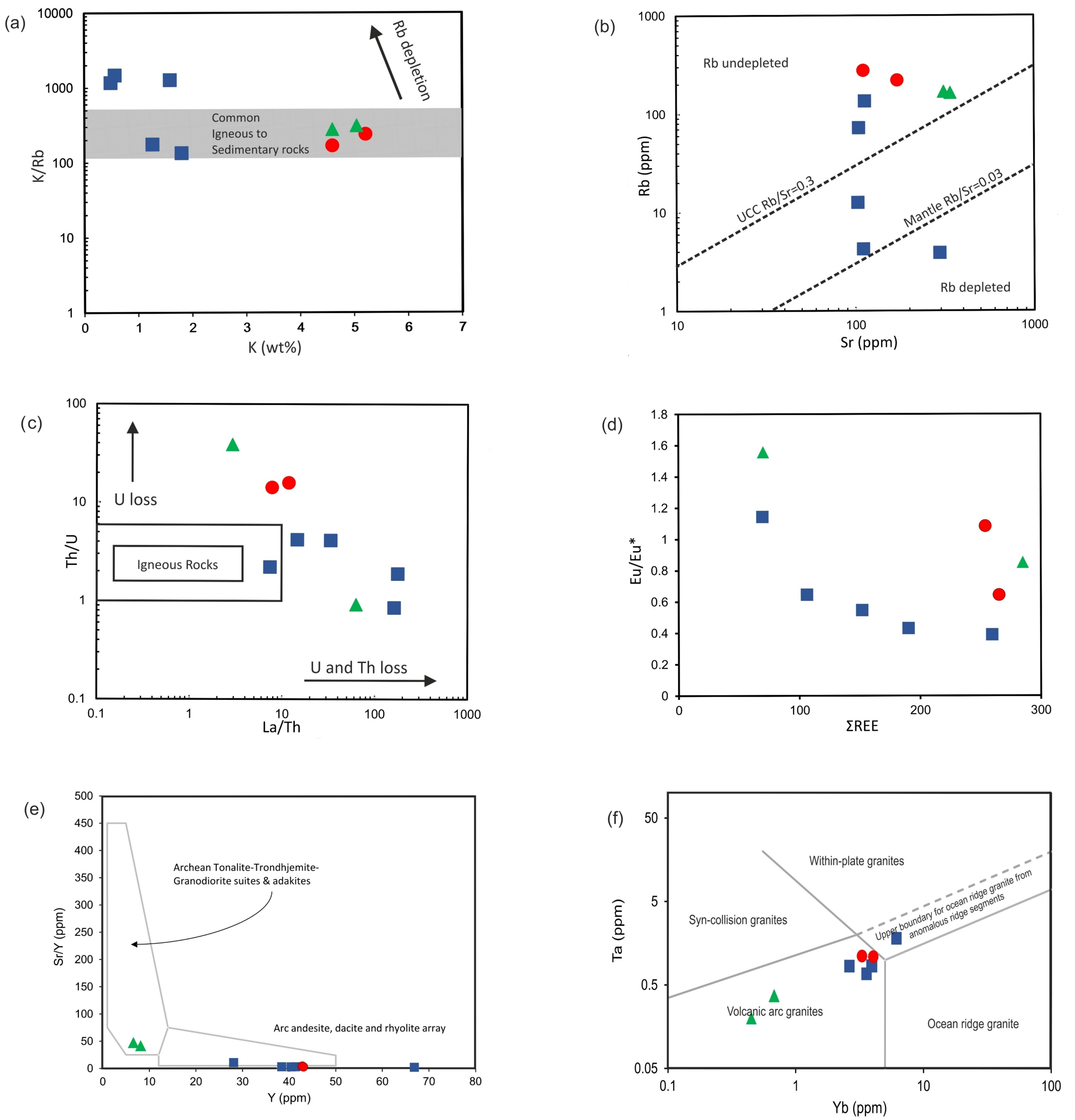
(a)
Rb depletion
Common Igneous to Sedimentary rocks
K/Rb
K (wt%)
(b)
Rb undepleted
UCC Rb/Sr=0.3
Mantle Rb/Sr=0.03
Rb depleted
Rb (ppm)
Sr (ppm)
(c)
U loss
Igneous Rocks
U and Th loss
Th/U
La/Th
(d)
Eu/Eu*
ΣREE
(e)
Archean Tonalite-Trondhjemite-Granodiorite suites & adakites
Arc andesite, dacite and rhyolite array
Sr/Y (ppm)
Y (ppm)
(f)
Within-plate granites
Syn-collision granites
Upper boundary for ocean ridge granite from anomalous ridge segments
Volcanic arc granites
Ocean ridge granite
Ta (ppm)
Yb (ppm)

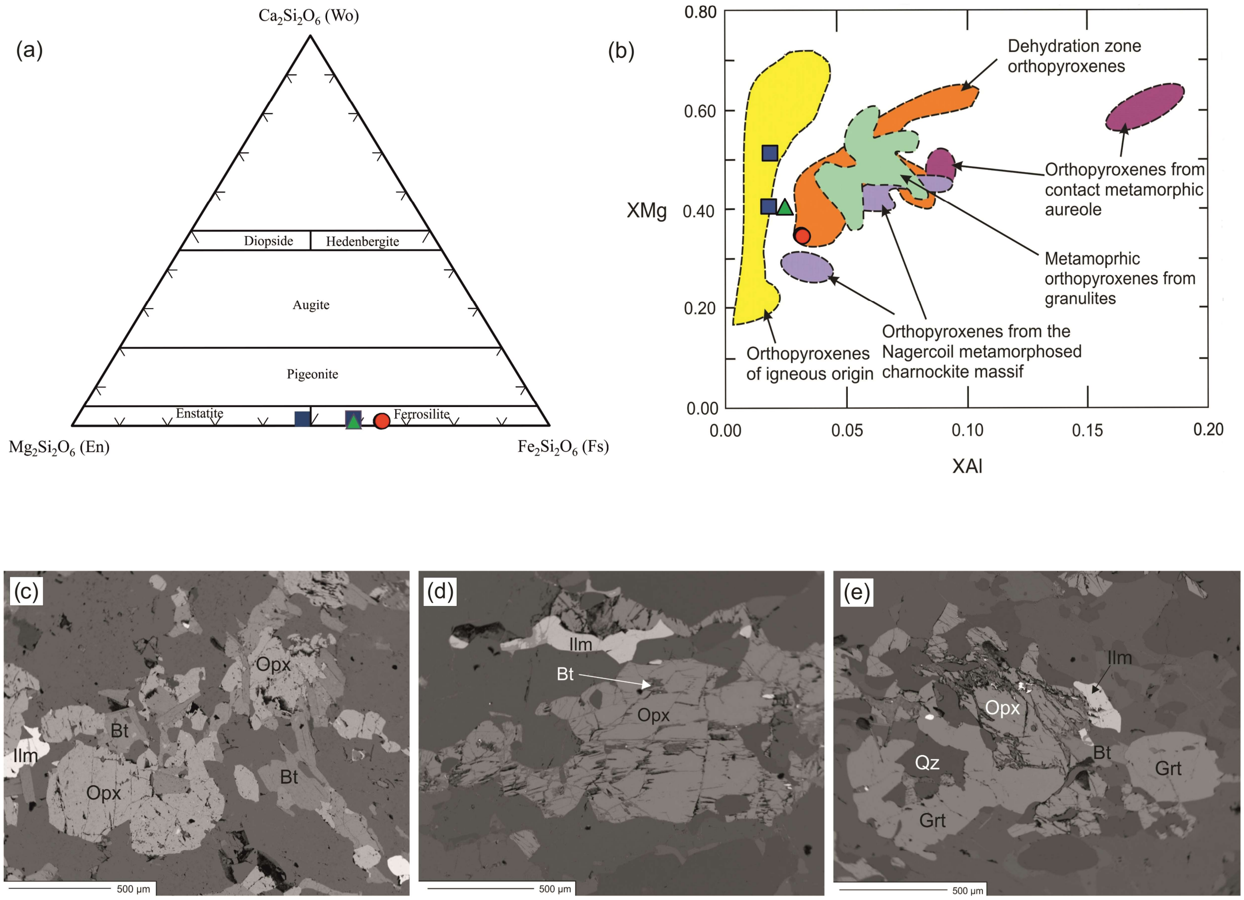
(a)
$Ca_2Si_2O_6$ (Wo)
Diopside
Hedenbergite
Augite
Pigeonite
Enstatite
Ferrosilite
$Mg_2Si_2O_6$ (En)
$Fe_2Si_2O_6$ (Fs)
(b)
Dehydration zone orthopyroxenes
Orthopyroxenes from contact metamorphic aureole
Metamoprhic orthopyroxenes from granulites
Orthopyroxenes from the Nagercoil metamorphosed charnockite massif
Orthopyroxenes of igneous origin
XMg
XAl
0.00
0.20
0.40
0.60
0.80
0.00
0.05
0.10
0.15
0.20
(c)
Opx
Bt
Ilm
Opx
Bt
500 µm
(d)
Ilm
Bt
Opx
500 µm
(e)
Ilm
Opx
Qz
Bt
Grt
Grt
500 µm

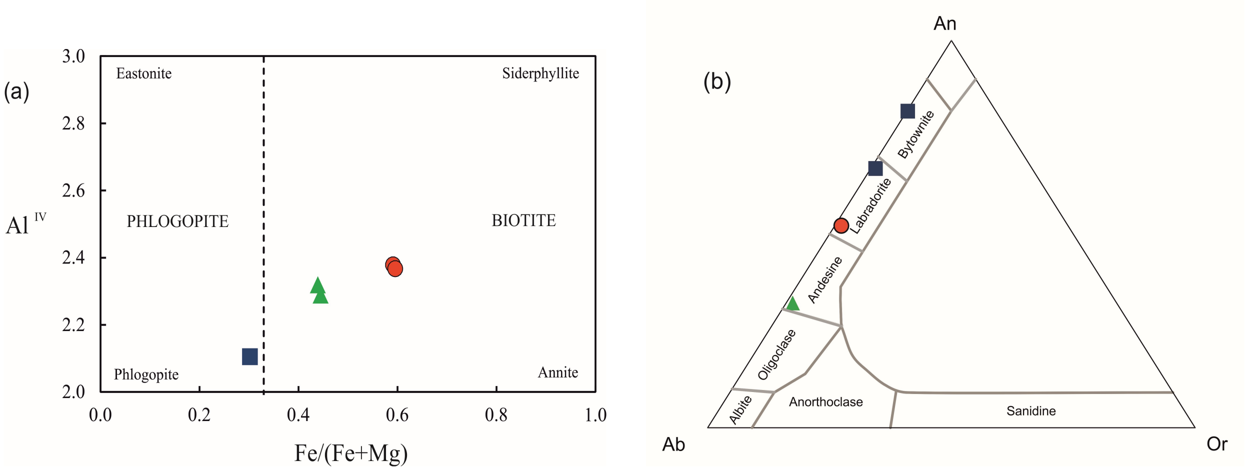
(a)
3.0
2.8
2.6
2.4
2.2
2.0
Al IV
0.0
0.2
0.4
0.6
0.8
1.0
Fe/(Fe+Mg)
Eastonite
Siderphyllite
PHLOGOPITE
BIOTITE
Phlogopite
Annite
(b)
An
Ab
Or
Bytownite
Labradorite
Andesine
Oligoclase
Albite
Anorthoclase
Sanidine

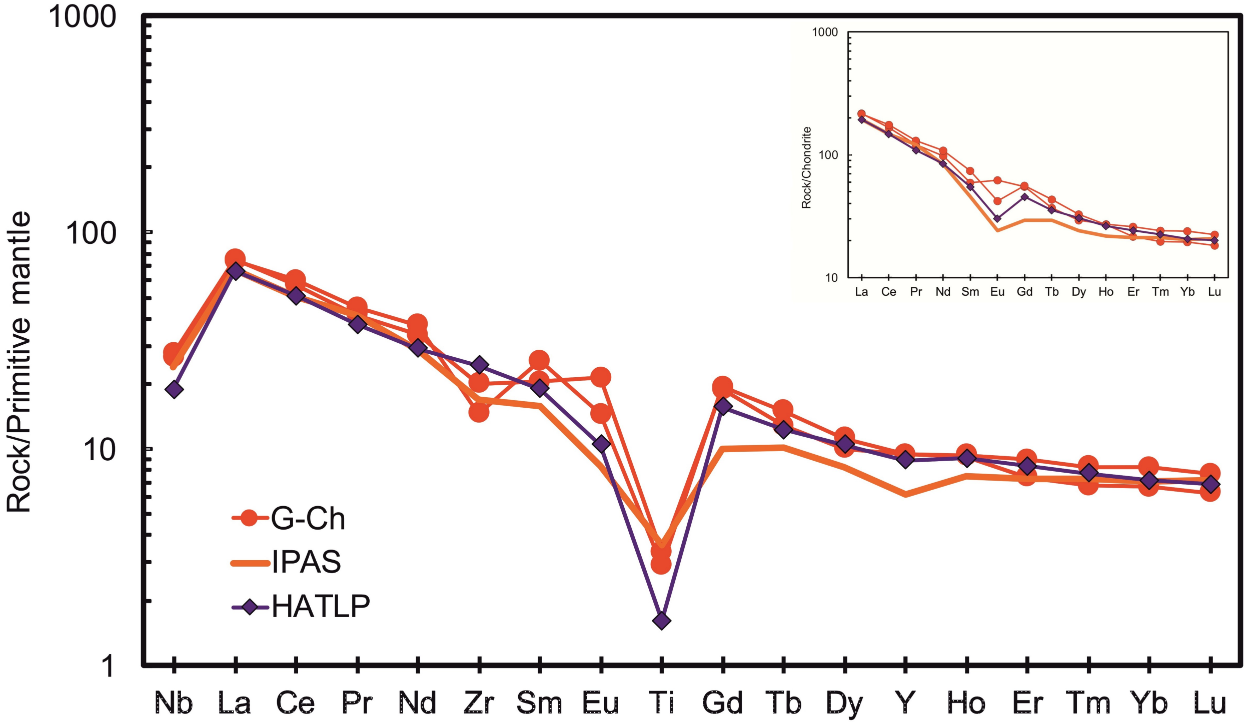

1000
100
10
1
Rock/Primitive mantle
Nb
La
Ce
Pr
Nd
Zr
Sm
Eu
Ti
Gd
Tb
Dy
Y
Ho
Er
Tm
Yb
Lu
G-Ch
IPAS
HATLP
1000
100
10
Rock/Chondrite
La
Ce
Pr
Nd
Sm
Eu
Gd
Tb
Dy
Ho
Er
Tm
Yb
Lu

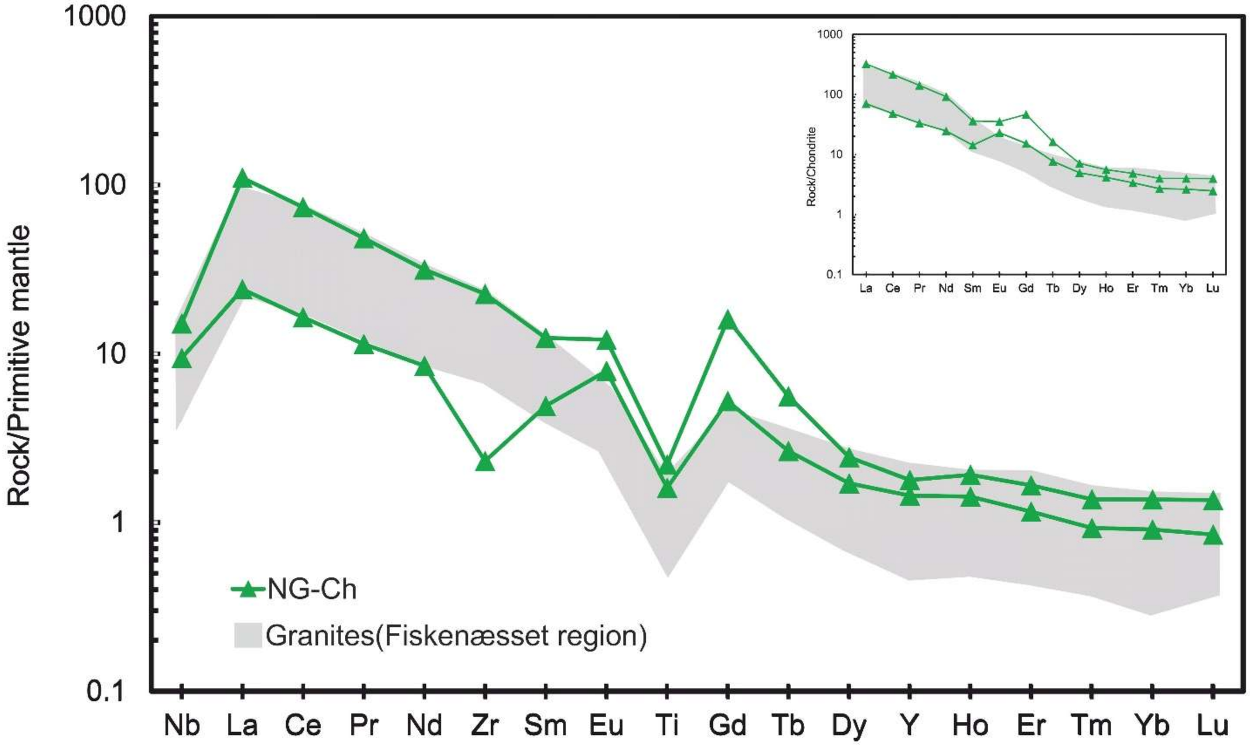
1000
100
10
1
0.1
Rock/Primitive mantle
Nb
La
Ce
Pr
Nd
Zr
Sm
Eu
Ti
Gd
Tb
Dy
Y
Ho
Er
Tm
Yb
Lu
NG-Ch
Granites(Fiskenæsset region)
1000
100
10
1
0.1
Rock/Chondrite
La
Ce
Pr
Nd
Sm
Eu
Gd
Tb
Dy
Ho
Er
Tm
Yb
Lu